https://doi.org/10.1016/j.tws.2022.110444

Review on blind bolted connections to concrete-filled steel tubes

Y.L. Li[1], T.M. Chan[1] and X.L. Zhao[1]*
[1]Department of Civil and Environmental Engineering, The Hong Kong Polytechnic University, Kowloon, Hong Kong, China
(*corresponding author: xiao-lin.zhao@polyu.edu.hk)

Abstract: Development of blind bolting systems offers an alternative solution of jointing steel beams to concrete-filled steel tubular (CFST) columns that only allow one-side access. This paper presents a critical review on recent studies about the blind bolted connections to CFSTs representing the tension zone in a beam-to-column joint. Various types of blind bolts have been proposed to improve their tensile behavior in CFSTs by implementing innovative interlocking mechanisms to tube wall and anchoring techniques in concrete. Experimental and finite element (FE) studies were first reviewed in this paper. Tensile behavior of a single bolt or a group of bolts in CFSTs was investigated by one-side or two-side pullout test. Its performance depended on a wide range of parameters, such as bolt type, bolt size, bolt grade, bolt layout, tube size, tube yield strength, concrete strength and embedment length. In FE simulations, modeling of concrete using concrete damage plasticity model was reviewed in detail to provide insights for an accurate FE analysis. Theoretical models for the tensile behavior of blind bolted connections to CFSTs were then reviewed. Strength and stiffness of a connection are mainly contributed by the tube face wall bearing effect, the anchorage in concrete and the elongation of bolts. Finally, potential research directions for future studies were suggested for blind bolted connections. In general, this jointing technique has a broad prospect to achieve a semi-rigid or even a rigid connection in beam-to-CFST joints.
Keywords: Anchored blind bolt; CFST; Anchorage; Pullout test; concrete damage plasticity model; Theoretical model

1. Introduction

Blind bolting system has been successfully used in steel closed sections that only allows one-side access. The blind bolting mechanisms are generally classified as three types [1]: (1) flowdrill drilling with the bolt and hole being threaded; (2) expansive sleeves for interlocking (e.g., Hollo bolt [2], MolaBolt [3]; (3) folded washer for interlocking, such as Huck Ultra-Twist bolt [4], Ajax ONESIDE blind bolt [5], and Blind Bolt [6]. Apart from these commercially available products, researchers also invented various types of blind bolts, to name a few, slip-critical blind bolt [7], reverse mechanism Hollo bolt [8], T-head square-neck one-side bolt [9]. Most of these blind bolts are claimed to have a comparable strength to the standard bolt.

Concrete-filled steel tubular (CFST) columns are widely applied in structures owing to its advantages of high strength, high ductility and desirable seismic performance [10]. A steel I-beam to CFST column joint could be classified as simple, semi-rigid or rigid depending on its moment-rotation response. In engineering practice, welded connection is most commonly used to achieve a rigid joint [11]. Nevertheless, on-site welding requires skilled manpower and it is difficult for quality control. In recent decades, blind bolted connections to CFSTs were under intensive research and various methods have been proposed to increase the rigidity, including setting binding bars, internal diaphragms, external channel sections [12], welding cogged bars [13] and using anchored blind bolts. Among them, the anchored blind bolt would be the most promising approach because it can be manufactured as a standard product and does not need welding.

A typical blind bolted beam-to-CFST joint with extended end plate is shown in Fig. 1. Because of the infilled concrete, deformation in the compression zone is negligible comparing to that in the tension zone. Based on the component concept, the tension zone could be simulated by a T-stub-to-CFST connection under tensile load. Furthermore, the bolt and tube behaviors are isolated by using a rigid T-stub. Behavior of a single bolt or a group of bolts connected to CFSTs is mainly governed by the bending of tube face wall and the anchorage effect in concrete. The behavior of tube face wall bending in steel hollow or open sections was specified in some design guides (e.g., CIDECT Design Guide No.9 [14]) using yield line method. For anchorage effect, concrete design standard [15] covered the design for anchoring in concrete and the failure modes for anchors include steel failure, pullout, concrete breakout, concrete splitting, side-face blowout, and bond failure. However, due to the complex interaction between steel tube, concrete and anchor, the behavior of blind bolted connection is certainly different from that of individual hollow section or concrete anchorage. During the last decades, extensive efforts have been devoted to understand the performance of blind bolted connections and various types of anchored blind bolts have been invented and investigated. Cabrera et al. [16]

and Tizani et al. [17] reviewed the studies on Extended Hollo Bolt (EHB) connections as will be discussed in Section 2.4, but they did not cover other types of blind bolts.

This paper presents a review on current and previous studies about blind bolted connections including a single bolt and a group of bolts connected to CFSTs (Fig. 1). Research on beam-to-column joints was not covered in this paper. Most of the studies were conducted during the past ten years indicating that the research intensity for this topic is surging. This review paper summarizes the existing experimental, finite element (FE) and theoretical investigations and provides suggestions for future studies. If not specified, the steel tube in this paper refers to square carbon steel tube.

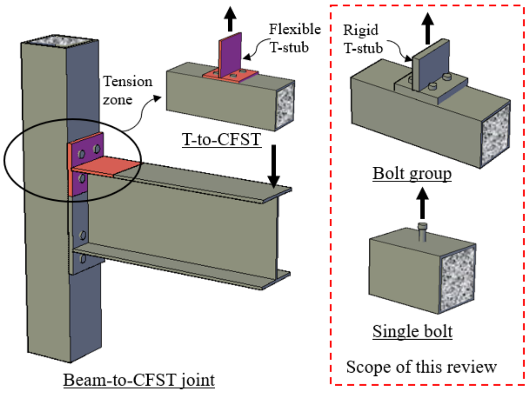

Fig. 1 Blind bolted connection.

2. Experimental studies on blind bolted connections

2.1 Blind bolt

Various types of blind bolts have been used for connections to CFSTs as shown in Fig. 2. Hollo bolt is a commercially available product initially for connections to closed hollow sections. A Hollo bolt is consisted of a collar, a cone with grooves, an expansive sleeve and a bolt shank (Fig. 2 (a)). Tizani's group at the University of Nottingham proposed to use an extended bolt shank with a headed anchor that is threaded onto the shank end (Fig. 2(b) to enhance the anchorage of Hollo bolt in concrete. Jeddi and Sulong [18] further proposed to add one more extensive sleeve and cone to the extended Hollo bolt as shown in Fig. 2(c). Ajax one-side bolt, which is featured as having a split step-washer, is another prevalent type in blind bolt market (Fig. 2(d)). With the help of a special installation tool, the folded washer is inserted through the hole and then unfolds to bare on the inner surface. Research group from the University of Melbourne [19] modified the Ajax bolt by replacing the bolt shank with a high-strength threaded rod with an anchor at end and called it as Ajax anchored bolt (Fig. 2(e)). Subsequently, this group proposed to set two anchors in the bolt to increase the stiffness of the connection as shown in Fig. 2(f) [20]. Besides the Hollo bolt, Ajax bolt and their variants, an anchored T-bolt was recently proposed in Sun et al. [21] as shown in Fig. 2(g), which consists of a T-head, an extended bolt shank and an anchor at end. The bolt is inserted into a slotted hole and then turn 90° so that the T-head bears on the inner wall.

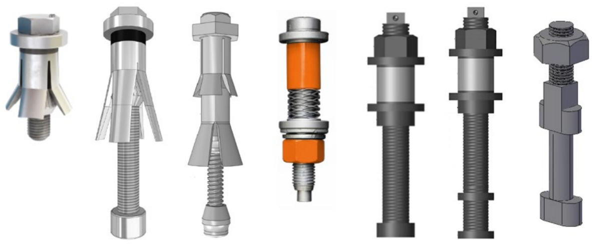

(a) (b) (c) (d) (e) (f) (g)

Fig. 2 Blind bolts used for connections to CFST: (a) Hollo bolt; (b) Extended Hollo bolt (EHB); (c) Double-headed extended Hollo bolt (DEHB); (d) Ajax one-side bolt; (e) Ajax anchored bolt; (f) Double-headed Ajax bolt; (g) Anchored T-bolt.

For Hollo and Ajax bolt types, an over-sized bolt hole is required to allow the sleeve or folded washer to be inserted into the closed section. The bolt shank diameter is smaller than that of a normal bolt. Anchored T-head bolt has the same cross-section with normal bolt but a slotted hole is compulsory in the CFST wall. The stadium-shape anchor in anchored T-head bolt generally provides a larger anchoring area in concrete than that of round anchors. However, the slotted hole in face wall may deteriorate the bearing strength of tubes. Experimental and FE studies reviewed in this paper are summarized in Table 1 and will be introduced in the subsequent parts of this section and Section 3.

Table 1 Summary of experimental and FE studies on blind bolted connections to CFST.

Data source	Specimen type	Loading type	Cross-section	Methodology
Hollo Bolt				
Li and Zhao 2022 [22]	Bolt group	Monotonic tension	Square	Test
Tan et al. 2019 [23]	Bolt group	Monotonic tension and shear	N/A	Test
Extended Hollo bolt				
Pitrakkos et al. 2012 [24]	Single bolt	Monotonic tension, preload	Square	Test
Pitrakkos et al. 2021 [25]	Single bolt	Monotonic tension and shear	Square	Test
Cabrera et al. 2020 [26]	Single bolt	Monotonic tension	Square	FEM
Debnath and Chan 2021 [27, 28]	Single bolt	Monotonic tension	Square	FEM
Debnath and Chan 2022 [29]	Single bolt	Monotonic tension	Square	Test
Debnath and Chan 2022 [30]	Single bolt	Monotonic shear	Square	Test
Tizani et al. 2014 [31]	Single bolt	Fatigue tension	Square	Test
Pascual et al. 2015 [32, 33]	Single bolt	Thermal behavior	Square	Test, FEM
Cabrera et al. 2021 [34]	Single bolt	Preload in bolt	Square	Test, FEM
Tizani and Pitrakkos 2015 [35]	Bolt group	Monotonic tension	Square	Test
Double-headed Hollo bolt				
Jeddi et al. 2018 [18]	Single bolt	Monotonic tension	Square	Test
Ajax anchored bolt				
Tan et al. 2019 [23]	Single bolt	Monotonic tension and shear	N/A a	Test
Oktavianus et al. 2015 [36]	Single bolt	Monotonic tension	Circular	Test, FEM
Agheshlui et al. 2016a [37]	Single bolt	Monotonic tension	Square	Test, FEM
Agheshlui et al. 2016b [38]	Bolt group	Monotonic tension	Square	Test, FEM
Double-headed Ajax bolt				
Oktavianus et al. 2017a [39]	Single bolt	Cyclic tension	Circular	Test, FEM
Pokharel et al. 2019 [40]	Single bolt	Cyclic tension	Square	Test, FEM
Oktavianus et al. 2017b [41]	Bolt group	Cyclic tension	Circular	Test, FEM
Pokharel et al. 2021 [42]	Bolt group	Cyclic tension	Square	Test, FEM
T-bolt				
Sun et al. 2021a [21]	Beam-to-column	Monotonic load at beam end	Square	Test
Sun et al. 2021b [43]	Beam-to-column	Cyclic load at beam end	Square	Test
Ng et al. 2022 [44]	Single bolt	Monotonic tension	Square	Test, FEM
CFST tube face wall				
Elamin 2014 [45]	Tube face wall	Monotonic tension	Square	Test, FEM
Mahmood et al. 2014 [46]	Tube face wall	Monotonic tension	Square	Test, FEM
Tizani et al. 2020 [47]	Tube face wall	Monotonic tension	Square	Test, FEM
Li and Zhao 2022 [22]	Tube face wall	Monotonic tension	Square	Test, FEM

2.2 Experimental setup

In order to investigate the structural behavior of a single bolt or a group of bolts connected to CFSTs, different experiment setups were adopted by researchers. One-side pull-out test was the most commonly used test on single bolt as shown in Fig. 3(a). The CFST is set against two thrust blocks connected to a test frame or strong floor. The tested bolt is pulled out by the rigid end plate that is connected to the actuator [29, 37]. In some studies, the steel tube was replaced by a reusable rigid steel box as shown in Fig. 3(b) to isolate the bolt behavior [48]. For test on bolt group, a rigid T-stub is widely used and the web of T-stub is gripped by the test machine. In some studies [22, 35], two T-stubs were used to achieve a symmetrically both-side tension as shown in Fig. 3(c), whereas a single-side tension setup similar as Fig. 3(a) was also adopted [18]. A pure shear experiment setup was reported in Pitrakkos et al. [25] as shown in Fig. 3(d). Furthermore, Pitrakkos et al. [25] designed a rig for bolts under combined tension and shear (Fig. 3(e)), in which a reusable steel-box assembly was chosen. Various tensile-to-shear load ratio could be achieved by adjusting the testing angle. Tan et al. [23]

proposed another setup to simultaneously apply tension and shear loads as shown in Fig. 3(f), in which the tension load is applied by two horizontal jacks and the shear force is applied by the downward load through a compact H-section. Debnath and Chan [30] proposed a pure shear test rig for Extended Hollo Bolts as shown in Fig. 3 (g) where the shear force was applied through two rigid plates. This experimental setup could reasonably simulate the shear force in the bolts in a beam-to-column joint. It is necessary to mention that the experimental setups of Fig. 3(b, e and f) only test the behavior of bolt anchored in concrete and the steel tube is not included.

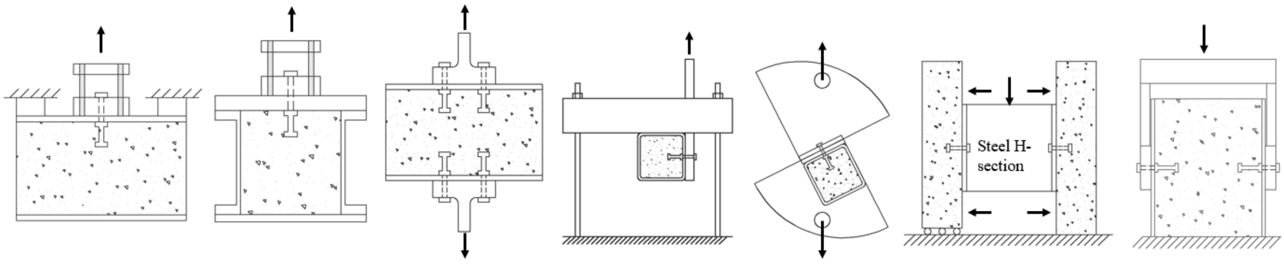

Fig. 3 Experimental setup: (a) One-side pull-out test for single bolt (Agheshlui et al. 2016 [37]); (b) One-side pull-out test with rigid tube (Pitrakkos and Tizani 2013 [48]); (c) Double-side tension test for bolt group (Li and Zhao 2022 [22]); (d) Pure shear test (Pitrakkos et al. 2021 [25]); (e) Combined tension and shear test with adjustable testing angle (Pitrakkos et al. 2021 [25]); (f) Combined tension and shear test (Tan et al. 2019 [23]); (g) Pure shear test (Debnath and Chan 2022 [30]). (Note: the bolt illustrated could be any type)

LVDTs were commonly used to measure the displacements at points with interest such as end plates, tube face walls, and supports. In some studies, the displacement recorded by test machine was directly used as the total displacement (e.g., double-side tension test in Li and Zhao [22]). In order to measure the slip of bolt, Pitrakkos and Tizni [48] proposed a method to measure the displacement at the unloaded bolt head in which a hollow stud was embedded in concrete to ensure an access to the unloaded end of bolt and a similar method was also proposed by Jeddi and Sulong [18]. Conventional strain gauges were used to measure the strain on bolt shank surface as shown in Fig. 4(a), in which the threads were milled off. Furthermore, a KYOWA bolt gauge as shown in Fig. 4(b) [49] that can be inserted into the predrilled hole in bolt shank was invented and being used (e.g., Lee, Goldsworthy and Gad [50]). This bolt gauge was also used to measure the pretension load in bolts [48]. Small-size load cells were more common for the pretension load measurement and the so called "bolt load cell" is available in market [29, 34]. Besides the conventional tools, non-contact measuring techniques, such as Imetrum Video Gauges [24] and photogrammetry method [38] were also employed by some researchers for displacement and strain measurements.

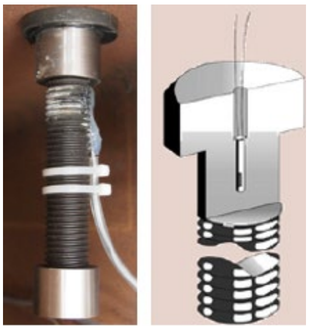

Fig. 4 Strain measuring techniques for bolts: (a) strain gauge on shank surface (Agheshlui 2016 [38]); (b) KYOWA bolt gauge [49].

2.3 Hollo bolt

2.3.1 Single bolt

In this paper, the sub-heading "Single bolt" refers to a single bolt anchored in concrete without the influence of steel tube. By using the experimental setup in Fig. 3(f) (with horizontal load only), Tan et al. [23] investigated the tensile behavior of Hollo bolt anchored in concrete (without encased tube). The whole bolt and its attached conical concrete cone with angles of 23° and 30° were pulled out as shown in Fig. 5. This concrete breakout failure was caused by the small embedment depth of bolt. Past studies on headed stud anchorage indicated that an embedment depth of 8~10 times of shank diameter could ensure the failure of connector happen before concrete breakage [51].

Amin et al. [52] tested the anchorage of Hollo bolts by the experimental setup in Fig. 3(b). Both the failure modes of concrete breakout and bolt fracture were observed. It is necessary to mention that the plate above the concrete block is thick in their study and would restrain the deformation of concrete.

Tan et al. [23] also tested Hollo bolts under combined tension and shear forces. During the experiment, tensile force was first applied to the prespecified value (0, 0.25, 0.5 or 0.75 of the tensile capacity) and the shear force (i.e., vertical load in Fig. 3(f)) was then applied to failure. Concrete breakout occurred for all the Hollo bolts. The relationship between the tensile force and the shear force was linear (Fig. 5), which was different from the elliptical shape of headed studs that was failed by stud fracture. The different interactive relationship is likely due to the distinct failure modes.

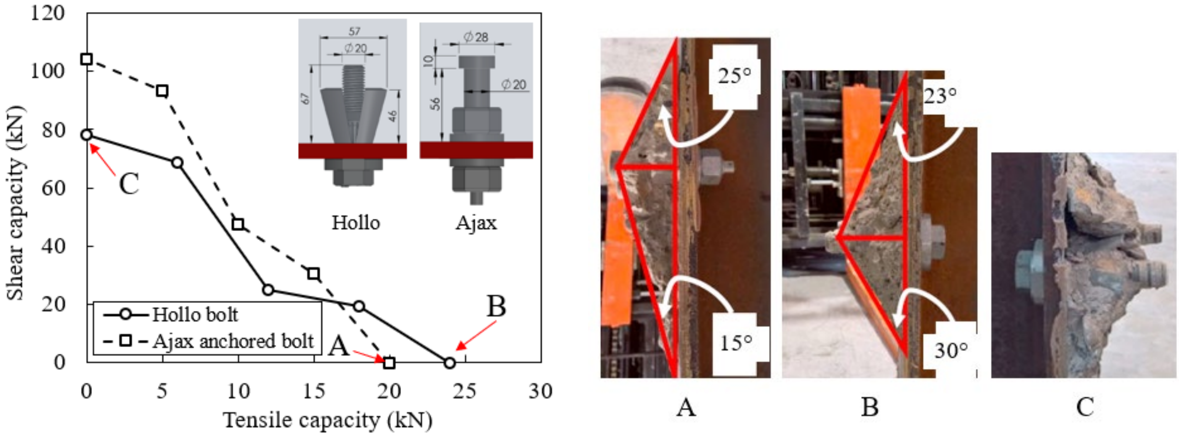

(a) (b)

Fig. 5 Interaction relationship between tension and shear capacity of Hollo bolt anchored in concrete (replotted from Tan et al. 2019 [23]): (a) interaction curves; (b) typical failure modes.

2.3.2 Bolt group connected to CFST

Li and Zhao [22] tested a stainless steel T-stub to stainless steel CFST connection under tensile load (Fig. 3(c)) and the bolt gauge and pitch were 100 mm. At the ultimate state, one of the four bolts was fractured resulting in a complete loss of strength and the flexible T-stub was in excessive deformation. During the experiment, with the increase in the deformation of T-stub, the loading state in Hollo bolt changed from tension to combined tension and shear.

Although the studies on single or a group of Hollow bolts connected to CFST is limited, extensive research has been reported for I-steel beam-to-CFST column joints using hollo bolt under monotonic or cyclic loads [53-55]. As this paper only focuses on single bolt or a group of bolts connected to CFSTs, which are basic components in a beam-to-column joint, the studies on beam-to-CFST column joints will not be covered.

2.4 Extended Hollo bolt (EHB)

EHB (Fig. 2(b)) was proposed by Tizani and Ridley-Elis [8] to improve the anchorage of the commercial Hollo bolt by extending its shank length and setting an anchor at the end. Extensive studies have been carried out for EHB connections, including the anchorage of bolt, bolt connected to CFST, T-stub to CFST connection containing a group of bolts and beam-to-column joints [56, 57]. Some of the studies were reviewed in the recent papers from Tizani's group [16, 17].

2.4.1 Single bolt

Pitrakkos and Tizani [48] designed an experimental setup to isolate the bolt component by setting a rigid face wall (Fig. 6) and the steel box consisted of two flat plates and two channel-profiles was reusable. The bolt was decomposed into three elements, i.e., internal bolt, expanding sleeve and bond & anchorage, as the sources of deformability (Fig. 6(c)). Monotonic pull-out tests were conducted on the EHB, Hollo bolt and threaded standard bolt with anchor. All the specimens were failed by the fracture of bolt shank indicating a full strength of bolt shank could be utilized. Owing to the additional anchorage and bond, EHB has an enhanced stiffness over the standard Hollo bolt. Concrete strength was found to noticeably affect the stiffness whereas internal bolt grade affected both stiffness and strength. EHBs with embedment depth of 4.0, 5.3 and 6.5 times bolt diameter (d_b) exhibited a similar stiffness and a minimum embedment depth of 4.0d_b was suggested for EHB.

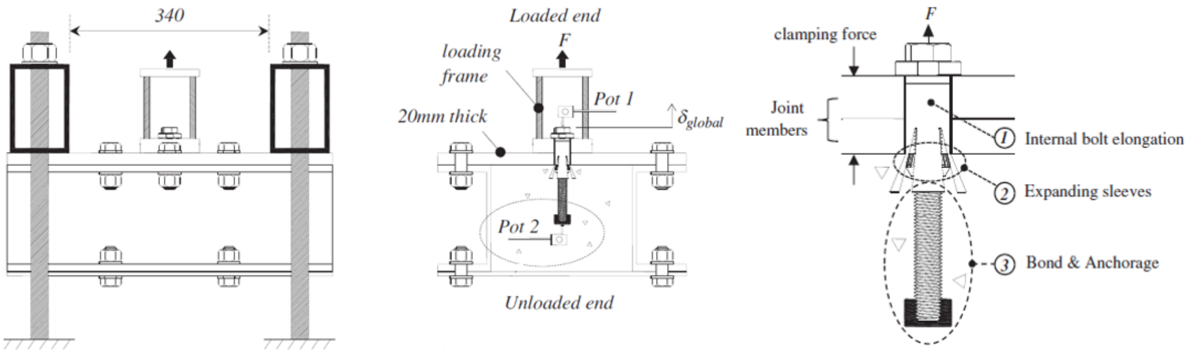

(a) (b) (c)

Fig. 6 Single bolt test for extended Hollo bolt in Pitrakkos and Tizani 2013 [48]: (a) Front view of setup; (b) Side view of setup; (c) Elements in EHB.

By adopting the reusable box in Fig. 6(b), Pitrakkos et al. [25] carried out experimental study on EHB subjected combined tension and shear force via the test rig shown in Fig. 3(e). A total of 13 specimens were reported and the normalized interaction relationship is replotted in Fig. 7. All the bolts failed by fracture. Necking was found for pure tension EHBs. Fracture surface for pure shear EHBs was flat and an inclined fracture surface was observed for EHBs under combined tension and shear. As shown in Fig. 7, the tensile strength of EHB is improved by a low level of shear force. Pitrakkos et al. [25] explained that the effective cross-section area of EHB under combined tension and shear was the area of shank and sleeve, which was larger than the effective area of EHB under pure tension that was the shank area. The interaction curve for EHBs is in a convex shape that differs greatly from the linear shape of Hollo bolt reported in Fig. 5. The major reason is the different failure modes, among which the failure mode was concrete breakout in Tan et al.'s [23] study whereas it was bolt shank failure in Pitrakkos et al.'s [25] study due to the usage of the rigid steel box.

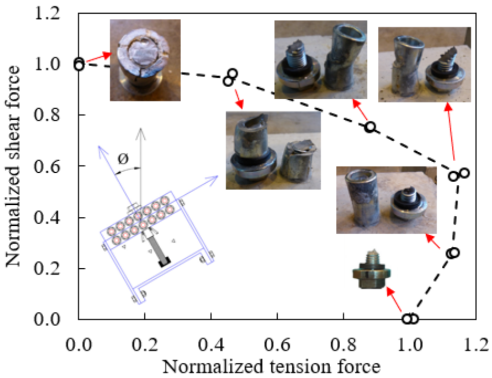

Fig. 7 Interaction relationship between tension and shear capacity of extended Hollo bolt anchored in concrete (replotted from Pitrakkos et al. 2021 [25])

2.4.2 Single bolt connected to CFST

Past studies on the behavior of single bolt tried to avoid the effect of steel tubes by either eliminating the tube (Fig. 3(f), [23]) or setting a rigid tube (Fig. 3(b), [48]). Nevertheless, the interaction of steel tube-to-concrete and steel tube-to-bolt exists in connections and some studies have been carried out on single bolt connected to CFSTs to investigate its overall behavior.

Pitrakkos [24] reported an exploratory pull-out test on EHB anchored in concrete (without tube), EHB connected to CFST and Hollo bolt connected to CFST and the force-displacement curves are replotted in Fig. 8. The strength and deformability of the connection was significantly enhanced by the steel tube. The steel tube contributes to the enhancement by bearing the expansive sleeves and restraining the outward deformation of the concrete. After the experiment, cracks were found on the concrete surface of the connection without steel tube but the cracking was not obvious for EHB connected to CFST. In addition, Hollo bolt connected to CFST showed the lowest strength and ductility among the compared connections, which confirmed the tremendous beneficial effect of the anchor.

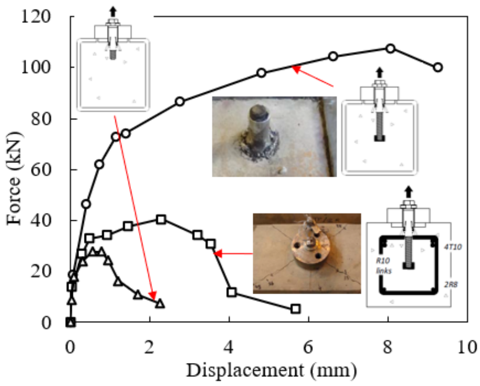

Fig. 8 Effect of steel tube and anchor on the force-displacement curves of EHB (replotted from Pitrakkos 2012 [24]).

Based on FE analysis, Cabrera et al. [26] investigated EHB connected to CFST and called it as "combined failure in tension" to highlight the influences of bolt and steel tube components. Specimen with low width-to-thickness tube exhibited a higher strength but the effect of width-to-thickness on the initial stiffness is insignificant. It is concluded that the concrete crushing accompanied with steel tube yielding occurred first and then the property of bolt in tension governed the strength. An analytic model was also proposed in this study, which will be reviewed in Section 4.3.3.

Debnath and Chan [27, 28] numerically investigated the tensile behavior of EHB in CFST connections. Effects of the parameters, including bolt embedment depth, bolt grade, bolt diameter, concrete grade, steel tube thickness and anchor size, on the tensile load-displacement curves were studied. There existed a sufficient embedment length and anchor size, beyond which their influences on EHB behavior were insignificant. It was concluded that the stiffness mainly depended on the tube width-to-thickness ratio, concrete grade, bolt diameter and embedment length, whereas bolt dimeter, concrete strength and embedment length mainly controlled the strength.

Debnath and Chan [29] tested single EHB connected CFST via a similar setup as Fig. 3(a). Depending on specimen parameters including bolt size, concrete strength, embedment length and tube thickness, three failure modes, namely bolt fracture, tube wall bending and combined failure of concrete crushing, tube wall bending and bolt sleeve fracture, were observed. By increasing embedment length and concrete strength, connection stiffness and strength were enhanced due to the increase in concrete crushing strength. A component method was proposed to estimate the load-displacement response of the connections and it will be reviewed in Section 4.3.

Debnath and Chan [30] experimentally investigated the performance of Extended Hollo bolts and standard Hollo bolts under pure shear loads via the setup in Fig. 3(g). All the bolts failed due to bolt shear fracture and concrete bearing failure was not observed. Beneficial effects of concrete infill on connection strength and stiffness were further confirmed. It was found that the shear strength of bolts could be fully utilized in the EHB-to-CFST connections. In general, effects of tube thickness, bolt embedment length and concrete strength on the shear capacity were insignificant as the failure modes were not altered by changing these parameters. Nevertheless, the stiffness was enhanced by 18% if changing the concrete strength from 39.1 MPa to 79.7 MPa. A larger bolt embedment length could reduce the load carried by the steel tube as more loads were transferred to the infilled concrete via bearing mechanism. A new formula was proposed to estimate the shear capacity of EHB, which included the contributions of bolt shank and sleeves.

Tizani et al. [31] conducted fatigue test for EHB, Hollo bolt and standard bolt connected to CFSTs. It was found that the fatigue performance of standard bolt (needs two-side access for installation) was superior than that of EHB and Hollo bolt but their performance at high stress level (i.e., nominal stress range-to- nominal design stress=0.9) was similar. A higher concrete grade improved the fatigue performance. It was concluded that the EHB fatigue life met the requirement in existing design rule for standard bolt.

Pitrakkos and Tizani [48] and Cabrera et al. [34] investigated the preload in Hollo bolt (or EHB) connected to SHSs and CFSTs. It was found that the hardening of infilled concrete does not influence the general relaxation trend but it extended the time of completing the most preload loss from 2 h to 24 h [34]. Fig. 9 summarizes the ratio of residual-to-initial preload in Hollo bolt (or EHB) from these studies. If accounting for the experimental discrepancies, the effects of concrete infill and the magnitude of initial preload on the preload loss ratio are insignificant. In Debnath and Chan's study [30], preload loss of Hollo bolt connected to hollow tube after 48 hours was 22%~24% for 8.8 grade and 9% for 10.9 grade.

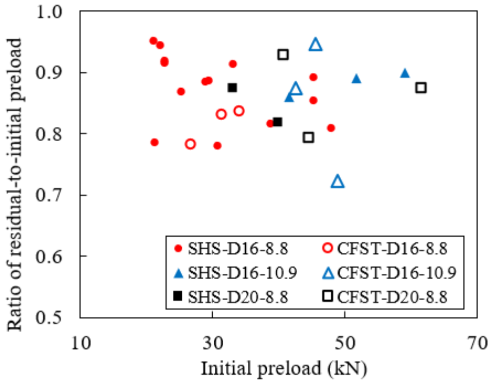

Fig. 9 Preload loss in Hollo bolt connected to SHSs and CFSTs (replotted from Pitrakkos and Tizani 2013 [48] and Cabrera et al. 2021 [34])

2.4.5 Bolt group connected to CFST

Tizani and Pitrakkos [35] studied the group behavior of EHBs connected to 200×10 mm CFSTs by using the double-side tension test with rigid T-stubs (2×2 bolts in each side, Fig. 3(c)). Effects of concrete strength, gauge distance (i.e., distance between bolts along the direction perpendicular to tube axis), pitch distance (i.e., distance between bolts along the tube axis) and bolt grade on the behavior of connections were discussed. All the specimens were failed by bolt shank fracture and the deformation of CFSTs was negligible. It was reported that the normalized force-displacement curves of connections with gauge distance of 90 mm and 120 mm were identical. This was because the stiffening effect provided by concrete infill surpassed the influence of bolt gauge [35]. The specimen with a larger bolt pitch exhibited a lower displacement at yield capacity than that of a specimen with a shorter pitch distance, but the comparison of displacement at ultimate capacity was opposite for them. An increase in concrete strength and bolt grade led to an enhancement of connection stiffness. In general, it was concluded that the EHB connection is suitable for semirigid or rigid moment connections.

2.5 Double-headed extended Hollo bolt

2.5.1 Single bolt

Further effect has been devoted to improve the anchorage of EHB, Jeddi and Sulong [18] proposed a new type of bolt as shown in Fig. 2(c), which consists two expansive sleeves. A comparison of the anchorage of EHB and Double-headed EHB (DEHB, also called "TubeBolt") was conducted in their study by pull-out test (similar as the setup in Fig. 3(a)). A 100 mm diameter hole was cut in the steel tube to eliminate the interaction between the infilled concrete and steel tube face wall. Fig. 10 replotted the load-slip curves of them as well as the photos of failure modes. Obviously, the stiffness and strength were greatly improved by setting two sleeves in the bolt. For DEHB, concrete breakout occurred leading to a dramatic loss of strength whereas concrete splitting was observed for EHB and it exhibited a more ductile behavior.

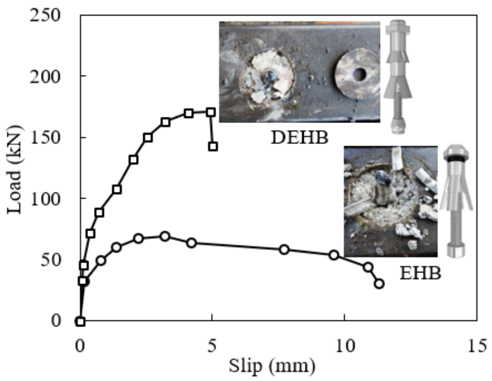

Fig. 10 Comparison of load-slip curves of DEHB and EHB anchored in concrete (Jeddi and Sulong 2018 [18])

2.5.2 Single bolt connected to CFST

Jeddi and Sulong [18] also investigated the behavior of double-headed EHB (DEHB) and EHB connected to CFSTs and the effects of end anchor, tube thickness (t) and bolt diameter (d_b) were studied. Load-slip curves of the tested specimens are replotted in Fig. 11. All the specimens were failed by the concrete cracking (or splitting) and the excessive deformation of steel tube, except specimen POT3 whose shank was ruptured. By comparing the curves of POT3 and POT4 to that in Fig. 10, the steel tube greatly increased the strength of the connection. Owing to the existence of the middle expansive sleeve, the end anchor contributed little to the strength and stiffness of DEHB, which accounted about 9% of total the strength. A larger tube thickness slightly increased the strength of the connections but its effect on the initial stiffness is negligible probably because the contribution of steel tube was not activated in initial loading process (POT3&4 vs. POT7&8 in Fig. 11). By increasing the bolt diameter from 16 mm to 20 mm, the strength of DEHB connection was greatly enhanced but the beneficial effect of EHB was insignificant, indicating DEHB could fully utilize its strength by providing a reliable anchorage in concrete. It was demonstrated that DEHB generally had a better performance than EHB in terms of strength and stiffness, but the deformability was slightly lower.

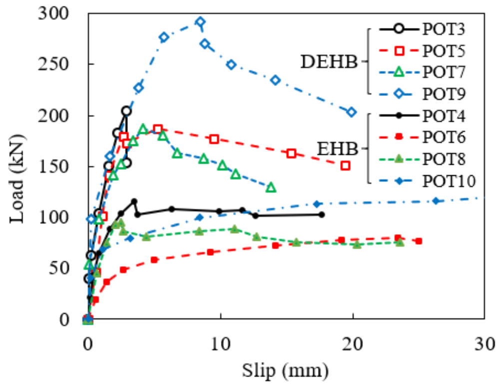

Fig. 11 Load-slip curves of DEHB and EHB connected to CFSTs (POT3&4: d_b=16 mm, t=8 mm; POT5&6: d_b=16 mm, t=8 mm, without end anchor; POT7&8: d_b=16 mm; t=6 mm; POT9&10: d_b=20 mm, t=8 mm; Jeddi and Sulong 2018 [18])

2.6 Ajax anchored bolt

2.6.1 Single bolt

The commercially available Ajax one-side bolt is not suitable for anchorage in concrete and researchers proposed to extend the bolt shank and set a headed stud at end as shown in Fig. 2(e). Tan et al. [23] also investigated the behavior of Ajax anchored bolt in concrete subjected to combined tension and shear using the setup in Fig. 3(f). The interaction curve of the Ajax anchored bolts is shown in Fig. 5, which shows a linear feature. Under pure tension, concrete breakout was observed and the angle of concrete cone was 15°~25°. Compared to Hollo bolt with the same shank diameter and embedment length, the shear capacity of Ajax anchored bolt is higher, but its tensile capacity is lower than the Hollo bolt. This is likely caused by the different shapes of their anchors leading to a different contacting area with concrete.

2.6.2 Single bolt connected to CFST

A series of studies have been conducted at the University of Melbourne, including the Ajax anchored single bolt, bolt group and double-headed Ajax bolt, which will be reviewed in this and the next section (i.e., Section 2.6 and 2.7).

Yao et al. [19] first explored the feasibility of using Ajax anchored bolt in concrete filled circular and square sections. For circular CFST, by setting a headed stud (i.e., anchor), the failure mode changed from tube wall yield and bolt pullout failure to bolt fracture with a significant increase in both strength and stiffness. The tube wall thickness had a pronounced influence for conventional Ajax bolt due to the load was resisted by the tube wall. However, it had a marginal effect for Ajax anchored bolt connection as the anchorage contributed most of the stiffness and strength. For square CFST, specimen with bolt located near the tube corner exhibited a stiffer behavior than that in the middle of tube.

Oktavianus et al. [36] experimentally and numerically investigated the pullout behavior of single Ajax anchored bolts embedded in circular CFSTs using the setup in Fig. 3(a). Based on FE analysis, load-displacement curves of the connection and its components (i.e., tube and anchor) were obtained as replotted in Fig. 12, in which "Anchor" refers to an Ajax anchored connection without the nut bearing on the tube wall, "Tube bearing" refers to a connection with Ajax bolt, and "Total" means an Ajax anchored bolt connection. The tensile resistance and stiffness are mainly contributed by the washer bearing on the steel tube wall and the headed anchor bearing on the concrete (i.e., anchorage). Initially, concrete anchorage contributed most of the stiffness, but anchorage's contribution decreased with the development of damage in concrete. For a given embedment length, decreasing the tube thickness (i.e., diameter-to-thickness ratio) or increasing the anchor size would increase the contribution of anchorage to the total strength and stiffness. A minimal concrete compressive strength of 40 MPa and embedment depth were suggested for this type of connection.

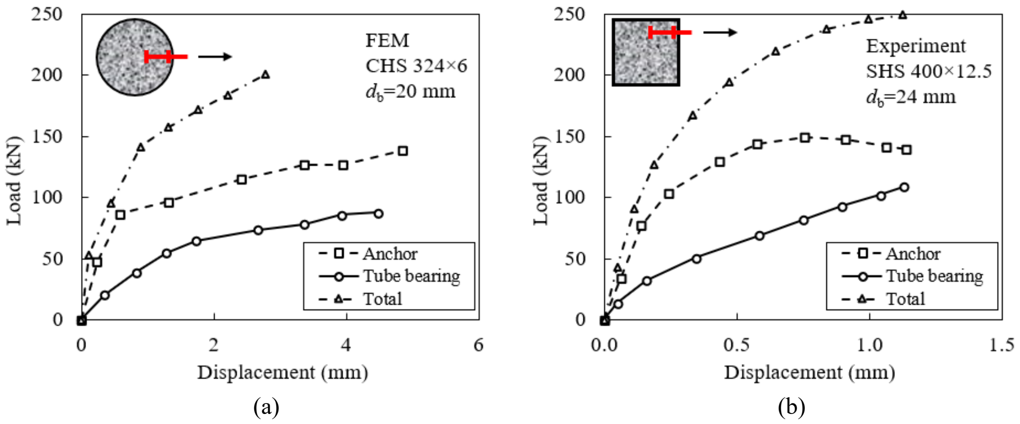

Fig. 12 Contributions of tube bearing effect and anchorage to the strength and stiffness of Ajax anchored bolt: (a) connected to circular CFST (Oktavianus et al. 2015 [36]); (b) connected to square CFST (Agheshlui et al. 2016 [37]).

Agheshlui et al. [37] investigated the tensile behavior of Ajax anchored bolt connected to square CFSTs. By measuring the strains at bolt shank, the loads resisted by anchorage effect and tube bearing effect were extracted as shown in Fig. 12(b). Similar as circular CFSTs, the stiffness and strength were mainly contributed by the anchorage during the initial loading process. With an increase in concrete damage and tube deformation, contributions from tube bearing started to increase. Their experimental results indicated that the bonding in bolt shank slightly affected the behavior of the connection. Furthermore, a connection with bolt in the middle of tube had a much lower stiffness and strength than that with bolt near the side wall. In the former case, a concrete cone was developed whereas a compressive strut was formed in the later case leading to an improvement in anchorage. It is necessary to mention that Tizani and Pitrakkos's study [35] found that the effect of bolt location (i.e., bolt gauge length) was insignificant, probably because the variation range of the gauge length was much smaller than that in the study of Agheshlui et al. [37].

2.6.3 Bolt group connected to CFST

By the one-side tensile test with rigid T-stub (Fig. 3(c) with one-side T-stub), Agheshlui et al. [38] studied the pullout behavior of groups of Ajax anchored bolts (1×2 or 2×2 layout) connected to CFSTs. It was found that the bolt diameter had an apparent effect on the tensile behavior, but the influence of pitch length was negligible. The load-displacement curve of a group of bolts is similar as that of an individual bolt. In addition, FE-based parametrical study was conducted to clarify the effects of concrete strength, tube thickness, bolt diameter, anchor size, gauge length, pitch length and embedment length on the connection behavior. Among them, concrete strength, bolt diameter and strut angle that is related to the embedment length and the distance between bolt and side wall (bolt gauge) had the most profound effects. A strut angle of 30°~45° was optimum for the formation of an efficient strut. Similar as the findings in single bolt, the anchorage dominated the connection behavior during the initial stage and the steel tube became more influential during the late loading stage.

2.7 Double-headed Ajax bolt

2.7.1 Single bolt connected to CFST

In order to increase the stiffness of the connections, a double-headed Ajax bolt was proposed by setting two anchors in the Ajax bolt as shown in Fig. 2(f). Oktavianus et al. [20] investigated the cyclic behavior of individual double-headed Ajax bolt connected to circular CFSTs whose diameter-to-thickness ratio is 48.1. Little stiffness degradation was observed for tested specimens under cyclic loads up to 60% of the nominal strength of bolt. Based on FE analysis, contribution of the anchors (1st and 2nd anchor) and tube to the connection capacity was clarified as shown in Fig. 13, including connections with normal concrete and steel fiber reinforced concrete. In general, the first anchor (H1) contributed more than the 2nd anchor (H2) and the tube wall. With the increase in load, the load resisted by the first anchor decreased due to concrete damage and the load carried by the 2nd anchor and the tube face wall increased. The degradation of the contribution from the 1st anchor occurred at a slower rate if using the fiber reinforced concrete as it provided tensile strength across the cracks. An optimal embedment length was also suggested in the study to achieve the highest stiffness.

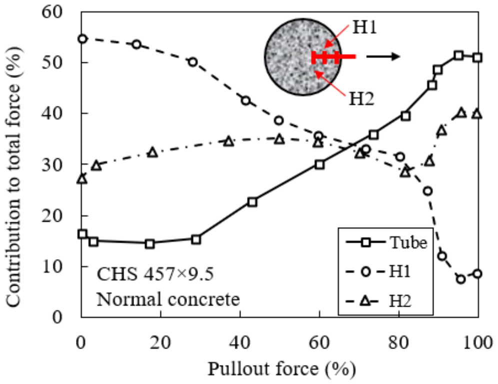

(a)

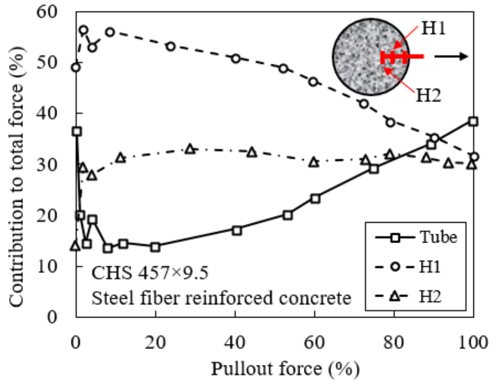

(b)

Fig. 13 Contribution of tube wall bearing (Tube), the first anchor (H1) and the second anchor (H2) to the pullout out force (FE results): (a) specimen with normal concrete; (b) specimen with steel fiber reinforced concrete. (replotted from Oktavianus et al. 2017 [20])

Cyclic performance of the double-headed Ajax bolt connected to square CFSTs was studied in Pokharel et al. [40] by pullout test similar as Oktavianus et al. [20] (Fig. 3(a)). The steel tube size was 400×12.5 mm and 400×10 mm, and the bolt was located at the 1/4 location of the tube face wall. The maximum amplitude of the cyclic loads was 60% of the nominal tensile capacity of the bolts. Degradation of the connection stiffness due to the cyclic loads was not observed in the experiments. FE results indicated that the contribution of the 1st anchor was prevalent at low load level, but the contribution of the 2nd anchor exceeded that of the 1st anchor at high load levels.

2.7.2 Bolt group connected to CFST

Oktavianus et al. [41] and Pokharel et al. [42] also investigated the cyclic behavior of a group of double-headed Ajax bolt connected to circular and square CFSTs, respectively, by using the one-side tensile test with rigid T-stubs. Similar as the results of single bolt connections, the stiffness degradation by cyclic load was insignificant. Parametrical study was performed by FE analysis to identify the parameter most affecting the connection behavior. In Oktavianus et al. [41], three types of specimens were tested as shown in Fig. 14, where TB for through bolt, SB for side bolt and DHAB for double-headed Ajax bolt. It was found that the through bolt and side bolt could greatly improve the connection stiffness (>100%). Owing to the inclination of the bolt (i.e., an angle between bolt axis and the force direction), the bolt was under combined tension and shear forces. Changing the orientation from 0° to 30°, 5% and 13% reductions of strength and stiffness were observed in FE analysis. In Pokharel et al. [42], the rigid T-stub was connected to square CFST by four double-headed Ajax bolts and one through bolt. The through bolt could improve the connection performance in terms of stiffness and cyclic deterioration. As expected, increasing bolt size and tube thickness could enhance the stiffness and strength. Nevertheless, the effect of concrete strength on the stiffness was not obvious.

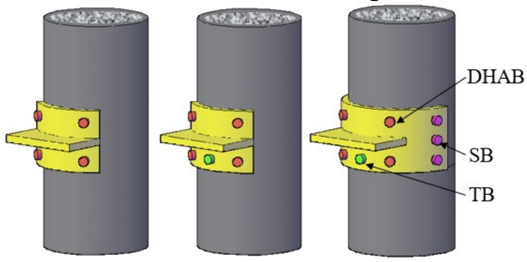

Fig. 14 Specimens tested in Oktavianus et al. 2017 [41].

2.8 Anchored T-bolt and its variants

Sun et al. [58] proposed a novel T-bolt for steel hollow sections and then modified the bolt for CFST connections by extending the shank and setting an anchor as shown in Fig. 2(g). Currently, no studies have been reported for the behavior of this anchored T-bolt under tension but a steel I-beam to CFST connection was tested under monotonic and cyclic loads [21, 43]. Pullout of anchored T-bolts with concrete fracture were observed in the tensile zone and the damage in bolt was not obvious. The tensile capacity was consisted of the bearing capacity of steel tube wall and the breakage resistance of the concrete cone whose inclination angle was set as 45°.

A T-bolt with ellipse bolt head was proposed in Wan et al. [59] and its shear behavior was experimentally and numerically investigated. Ng et al. [44] extended its application to CFSTs by adding one or two anchors. A total of five configurations of the anchored T-bolt (i.e., without anchor, one anchor, two anchors, reduced diameter of the extended shank, Fig. 15(a)) were tested in Ng et al. [44] by the one-side tensile test (Fig. 3(a)).

Pullout failure occurred for the bolts without anchor and bolt fracture or shear off failure happened for the bolts with anchors (Fig. 15(b)). As expected, the anchor could significantly enhance the stiffness and strength of the connection. However, experimental results showed that the bolt with a single anchor had a similar response to the bolt with double anchors. The diameter of the embedded shank affected the connection stiffness but its influence on strength was negligible. Sufficient embedment lengths were also suggested in their study, which depended on the bolt diameter. Based on FE analysis, the initial stiffness was not affected by tube thickness, although the stiffness at high load level increased as the tube thickness increased.

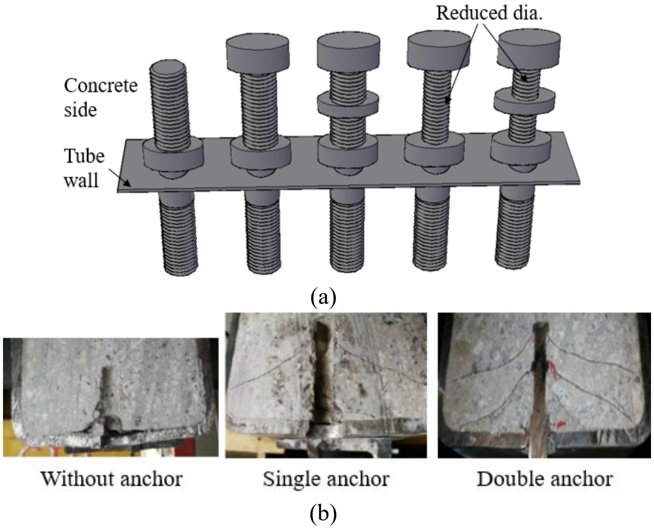

Fig. 15 Anchored T-bolted connection in Ng et al. 2022 [44]: (a) bolt type; (b) crack patterns in concrete

2.9 Behavior of CFST under tension

Elamin [60], Mahmood et al. [61] and Tizani et al. [47] used the so called "dummy bolt" to investigated the behavior of CFST under tensile loads. The dummy bolt was made from high strength steel achieving a strong bolt and weak tube to isolate the behavior of tube face bending. A typical specimen in Tizani et al. [47] is shown in Fig. 16 but the dummy bolt in Elamin [60] did not have the anchor. Based on experimental study in Elamin [60], it was found that the strength and stiffness of the connection increased with the increase in bolt gauge length, concrete strength and the decrease in tube width-to-thickness ratio. Tizani et al. [47] found that the failure process was anchorage failure followed by steel tube yielding and then the pullout of bolt. Concrete strength had a significant effect on the connection strength and stiffness. It said that the confinement provided by the steel tube could affect the connection behavior by influencing the strength of concrete, and the confinement was related to the width-to-thickness ratio and steel yield strength. Although rigid bolts were used in these studies, the contribution by concrete anchorage was not eliminated in the experiments and this is likely the reason that the concrete strength played a great role in the connection behavior.

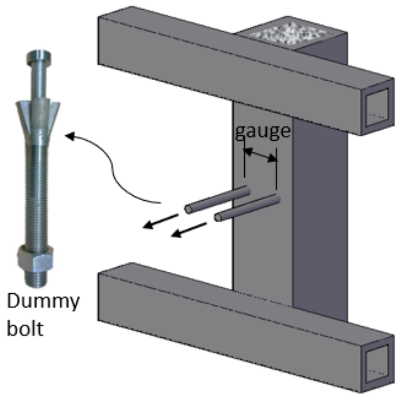

Fig. 16 Specimen with dummy bolts (Tizani et al. 2020 [47])

Li and Zhao [22] used the normal bolts to investigate the behavior of CFST under tension (Fig. 3(c) with 2×2 bolt layout. Since the bolt nut was directly bore on tube wall and no interaction existed between the bolt and concrete, the contribution of the tube was isolated. It was confirmed that the infilled concrete could greatly enhance the stiffness and strength as the concrete restrained the inward deformation of steel tubes. Experimental results indicated that tube thickness and bolt gauge greatly affected the connection behavior, but the influence of bolt pitch was negligible. At large deformation, obvious membrane effect was observed in the tube face wall.

2.10 Blind bolted connection under elevated temperatures

Under elevated temperatures, the stiffness and strength of steel will degrade and the material property degradation has been specified in relevant standards, such as EN 1993-1-2 [62]. A few studies have been conducted for blind bolted connections under elevated temperatures. Pascual et al. [32, 33] investigated the thermal response of EHB-to-CFST, Hollo bolt-to-CFST and Hollo bolt-to-SHS connections in fire. Steel tube size and bolt type slightly affected the temperature-time response but the existing of concrete could greatly reduce the increasing rate of temperature. In addition, an FE model was developed to simulate the heat transfer. You et al. [63, 64] and Wang et al. [65] experimentally investigated behavior of T-stubs connected by thread-fixed one-side bolts at elevated temperatures. As expected, the initial stiffness and tension strength were decreased whereas the ductility was increased with the increase in temperatures. It was found that the back-plate could increase the fire-resistance capacity of the connections. Eight full-scale blind bolted joints were tested to study their fire performance by Song et al. [66] and the blind bolted joints demonstrated very good performance in fire. Binding bars and steel tube type had moderate effects on the fire resistance but the effect of beam protection was significant. In general, effects of elevated temperature on the behavior of blind bolted connections are induced by affecting the properties of steel material.

2.11 Summary of extended Hollo bolt, Ajax anchored bolt and anchored T-bolt

Past studies introduced in previous sections have demonstrated the beneficial effect of the anchorage in enhancing the stiffness and strength of the connections. The main difference between extended Hollo bolt, Ajax anchored bolt and anchored T-bolt is the interlocking mechanisms. The interlocking between extended Hollo bolt and steel tube wall is complex involving the inclined sleeves and the concrete between the sleeves and tube wall. The inner nut surfaces of Ajax anchored bolt and anchored T-bolt are flat and could be directly bore on the steel tube wall. No direct comparison has been conducted for the behavior of these bolt types. In general, the load transfer between bolt and tube wall is more straightforward for Ajax anchored bolt and anchored T-bolt than that of the extended Hollo bolt. Special tools are needed for the installation of Ajax anchored bolt. Slotted holes are required for the anchored T-bolt and the slotted hole may reduce the bearing capacity between the T-head and tube wall. For for all these anchored blind bolts, over-sized holes are required to ensure the insertion of the anchors and sleeves/washers through the holes. Therefore, these bolts have their own unique features and a proper selection of the bolt type should be based on the requirement for the behavior, available techniques and cost of the bolts.

3. Finite element analysis on blind bolted connections

3.1 FE modeling for blind-bolted connection

As shown in Table 1, finite element (FE) analysis was widely used for blind-bolted connections to CFSTs. A reliable FE model needs to appropriately simulate the behavior of concrete (e.g., cracking, crushing and dilation), bolt, steel tube and the interactions between them, which involves high nonlinearity in geometry, material and contact. This paper only reviews the FE modeling based on commercial software ABAQUS [67] that was most widely used in connection simulations.

Solid element such as C3D8R (8-node linear hexahedral with reduced integration) was commonly used for concrete, bolt and tube and a fine mesh was adopted for the parts with complex stresses and high nonlinearity. Metal plasticity model was used for bolt and steel tube and the engineering stress-strain relation obtained from experiments needed to be converted to "true" stress-strain data for ABAQUS input. Concrete damage plasticity model was widely adopted for concrete constitutive model. Boundary conditions and loads were applied based on experimental setups. Owing to the complex interaction between the components (i.e., concrete, tube and bolt), contacts in Abaqus should be carefully defined and "surface-to-surface" contact was most commonly adopted in FE modeling. Both implicit (i.e., ABAQUS/Standard) and explicit (i.e., ABAQUS/Explicit) solution methods were used in past studies and the explicit method could avoid the convergence problem.

Pretension load is commonly applied to bolts by torque wrench to increase the stiffness in engineering practice. In ABAQUS/Standard, the pretention could be applied by "bolt load" method as documented in ABAQUS manual. A bolt load could be created by either applying a force or adjusting the bolt length. However, this method is not available for ABAQUS/Explicit and the "temperature load" method is prevalent in creating the pretension, which sets a thermal coefficient and temperature difference in bolt shank. Debnath and Chan [27] found that the pretension stresses in bolts created by "bolt load" and "temperature load" methods were very similar and the behaviors of bolt connections modeled by these two techniques were similar as well.

3.2 Concrete damage plasticity model

In existing FE studies for blind-bolted connections, concrete damage plasticity (CDP) model was most widely adopted as the constitutive model of concrete. This model could be applied for both plain and reinforced concrete subjected to monotonic, cyclic and dynamic loadings under low confinement. The CDP model in ABAQUS represents the inelastic behavior of concrete by using the concepts of plasticity and isotropic damage elasticity and mainly includes the defining of concrete plasticity, compressive behavior, tension stiffening and concrete damage [68].

Parameters for defining concrete plasticity includes the dilation angle (ψ), the ratio of biaxial-to-uniaxial strength (f_{b0}/f_c'), the ratio of the second stress variant on the tensile meridian to that on the compressive meridian (K_c) and flow potential eccentricities (ϵ). The dilation angle controls the dilation rate of concrete that induces interaction between concrete and its surrounded tubes. Sensitivity study may be needed for a proper identification of the dilation angle. Detailed explanations for these parameters could be found in the ABAQUS manual. Table 2 lists the default values of these parameters and suggested values in some typical FE studies [26, 27, 37, 69].

Table 2 Parameters for plasticity model

Ref.	ψ	f_{b0}/f_c'	K_c	ϵ
Default	N/A	1.16	2/3	0.1
Tao et al. 2013 [69] Debnath and Chan 2021 [27]	For circular section: $\begin{cases} 56.3(1-\xi_c), & \xi_c \le 0.5 \\ 6.672e^{\frac{7.4}{4.64+\xi_c}}, & \xi_c > 0.5 \end{cases}$ For rectangular section: 40°	$1.5(f_c')^{-0.075}$	$\dfrac{5.5}{5+2(f_c')^{0.075}}$	0.1
Agheshlui et al. 2016 [37]	36~40 °	1.16	2/3	0.1
Cabrera et al. 2020 [26]	55	1.16	0.8	0.1

Note: ζc is the confining factor equaling to $A_s f_y/A_c f_c$', where A_s is the cross-section area of steel tube, A_c is the cross-section area of concrete, f_y is the yield stress of steel and f_c' is the cylinder compressive strength of concrete.

Stress-strain relation of plain concrete under uniaxial compression is required for CDP model. Stress-strain model of unconfined concrete has been extensively studied including Popovics's model [70] and the models specified in standards (EC 2 [71], GB 50010 [72]). Mander et al. [73], Han et al. [74] and Tao et al. [69] proposed stress-strain models for steel-confined concrete. The stress-strain relation should be converted to stress-inelastic strain relation for ABAQUS input. It is necessary to keep in mind that the effective stresses control the size of the yield (or failure) surface and an adoption of confined stress-strain model in combination with damage variables may double-account the confining effect.

In ABAQUS, the post-failure behavior of cracked concrete is modeled with tension stiffening by either defining a stress-strain relation or specifying a fracture energy. The fracture energy method [75] is preferred for plain concrete and commonly used for CDP model in blind-bolted connections. Currently, various equations have been proposed for the fracture energy (G_f), such as CEB-FIP Model Code [76], Trunk et al. [77], FIB Bulletin 42 [78] and CEB-FIP Model Code [79] as summarized in Debnath and Chan [27], which are functions of concrete strength. In ABAQUS manual [68], G_f is suggested to be 40 N/m and 120 N/m for concrete with compressive strength of 20 MPa and 40 MPa, respectively.

Owing to the cracks and crush of concrete, the unloading stiffness at the point in the strain softening branch of a stress-strain curve is deteriorated and this elastic stiffness degradation is characterized by the damage variables (i.e., d_c for compressive and d_t for tensile damage). If the damage effect is not considered, the CDP model behaves as a plasticity model (Fig. 17), such as FE models in Han et al. [74] and Tao et al. [69]. In some studies, identification of the damage variable was not clearly stated. Agheshlui et al. [37] assumed d_c is equal to the ratio of the inelastic strain to the total strain capacity and d_t=0 and 0.99 for zero and ultimate displacement, respectively. Pokharel et al. [42] adopted d_c and d_t specified in Jankowiak and Lodygowski [80]. Waqas et al. [81] adopted the model of Birtel and Park [82], in which the plastic strain is assumed to be proportional to the inelastic strain with a constant of 0.7. By assessing existing experimental data on plain concrete under cyclic compression (Sinha et al. [83], Okamoto et al. [84], Tanigawa and Uchida [85], Bahn and Hsu[86]) and assuming the damage only occurs in the strain-softening branch of the uniaxial stress-strain curve, Eq. (1) is suggested to determine d_c (Fig. 18).

$$d_c = \begin{cases} 0 & ,\varepsilon_c \le \varepsilon_{co} \\ 1-\exp[-1.25(\dfrac{\varepsilon_c}{\varepsilon_{co}}-1)^{0.75}] & ,\varepsilon_c > \varepsilon_{co} \end{cases} \quad (1)$$

where ε_{co} is the strain at f_c' taken as $0.000937f_c'^{0.25}$ (where f_c' is compressive strength in MPa) as suggested in Popovics [70]. Debnath and Chan [27] assumed that 1-d_t is equal to the ratio of the tensile stress retention to the tensile strength (i.e., d_t=1-σ_t/f_t). The d_t-cracking displacement relationship could then be determined from the σ_t-cracking displacement curves that were, for example, specified in Hillerborg [87].

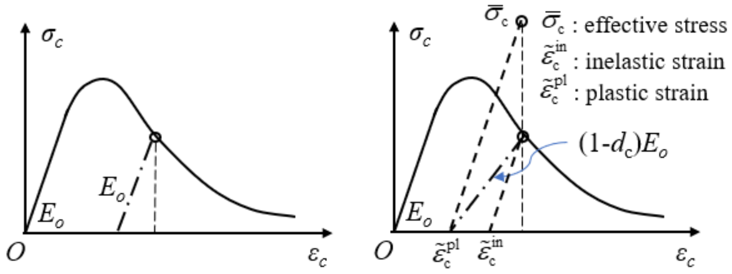

(a) (b)

Fig. 17 Compressive stress-strain relationship: (a) plastic model; (b) damage plastic model.

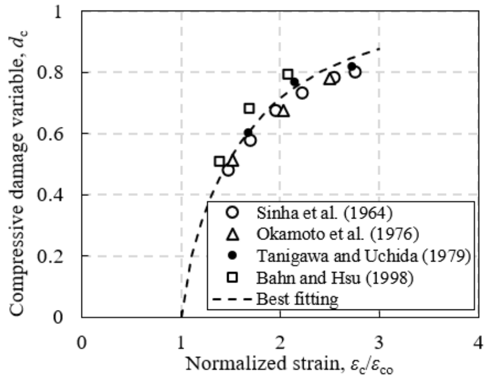

Fig. 18 Relationship between compressive damage variable and normalized strain.

4. Theoretical analysis

4.1 Components and forces in blind bolt

By reviewing existing studies, an individual blind bolt in CFST could be generally divided into three parts: locker, anchor and bolt shank. The stress distribution and force in bolt shank are illustrated in Fig. 19. The locker is under the bearing stress from tube face wall. The bolt shank embedded in concrete is subjected to bonding stress and the anchor is under anchoring stress. For Ajax anchored bolt and T-bolt and their variants, the surface of the locker (i.e., nut) is flat and it is tightly bore on the inner surface of tube wall, which is a straight forward interlocking. However, the interlocking mechanism is complex for Hollo bolt and its variants that involves the wedge effect and bearing effect (Fig. 19). In general, the connection is divided into multiple components represented by springs. After predicting the response of each components, the overall behavior of the connection could be obtained by assembling the springs. The strength and stiffness of the connection is mainly contributed by the tube bearing, bolt elongation and anchorage. Studies in Agheshlui et al. [37] concluded that the contribution of bonding in bolt shank is insignificant comparing with the contributions of tube bearing and anchorage. Theoretical models for blind bolted connections to CFSTs will be reviewed in the subsequent sections and a summary of the predictive formulas is shown in Table 3 for reference.

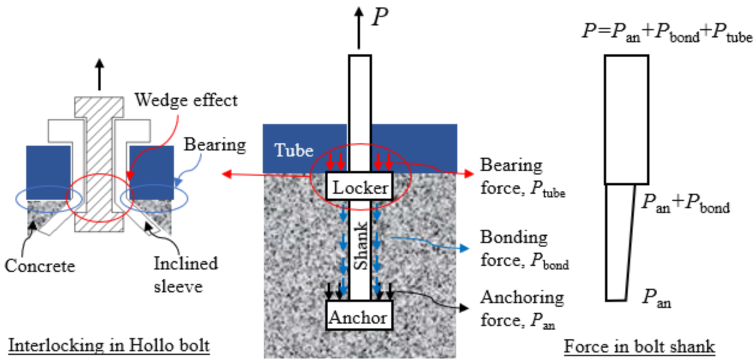

Fig. 19 Stress and force in anchored blind bolt.

Table 3 Summary of theoretical models.

Ref	Component	Design formula	Notations
Oktavianus et al. 2017 [39]	Bolt shank	$P_{\mathrm{y,bb}} = A_{\mathrm{bb}} f_{\mathrm{y,bb}}$; $P_{\mathrm{u,bb}} = A_{\mathrm{bb}} f_{\mathrm{u,bb}}$ $K_{0,\mathrm{bb}} = E_{0,\mathrm{bb}} A_{\mathrm{bb}} / L_{\mathrm{bb}}$ $K_{1,\mathrm{bb}} = E_{1,\mathrm{bb}} A_{\mathrm{bb}} / L_{\mathrm{bb}}$	$P_{\mathrm{y,bb}}$, $P_{\mathrm{u,bb}}$: yield and ultimate strength of blind bolt A_{bb}: effective area of blind bolt $f_{\mathrm{y,bb}}$, $f_{\mathrm{u,bb}}$: yield and ultimate strength of blind bolt $K_{0,\mathrm{bb}}$, $K_{1,\mathrm{bb}}$: initial and secondary stiffness of blind bolt $E_{0,\mathrm{bb}}$, $E_{1,\mathrm{bb}}$: initial and secondary elastic modulus from stress-strain curve $P_{\mathrm{u,tw}}$: ultimate capacity of tube wall
	Tube wall bearing	$P_{\mathrm{u,tw}} = 1.2 f_{\mathrm{u,tw}} \cdot \min\{d_{\mathrm{ws}} t_{\mathrm{tw}}, (d_{\mathrm{head}} + 2t_{\mathrm{ws}}) t_{\mathrm{tw}}\}$ $P_{\mathrm{y1,tw}} = 0.45 \cdot \frac{f_{\mathrm{y,tw}} / f_{\mathrm{u,tw}}}{350/430} \cdot P_{\mathrm{u,tw}}$ $P_{\mathrm{y2,tw}} = (f_{\mathrm{y,tw}} / f_{\mathrm{u,tw}}) \cdot P_{\mathrm{u,tw}}$ $K_{0,\mathrm{tw}} = \frac{\pi E_{\mathrm{tw}} t_{\mathrm{tw}}^2}{6(1-\nu^2) D_{\mathrm{o}}} \cdot (\frac{d_{\mathrm{ws}}}{d_{\mathrm{hole}}})^4$ $K_{1,\mathrm{tw}} = 20\% K_{0,\mathrm{tw}}$; $K_{2,\mathrm{tw}} = 6\% K_{0,\mathrm{tw}}$	$f_{\mathrm{y,tw}}$, $f_{\mathrm{u,tw}}$: yield and ultimate strength of tube wall steel d_{ws}: outer diameter of washer t_{tw}: thickness of tube wall d_{head}: diameter of bolt head $P_{\mathrm{y1,tw}}$, $P_{\mathrm{y2,tw}}$: first and second yield capacity of tube wall $K_{0,\mathrm{tw}}$, $K_{1,\mathrm{tw}}$, $K_{2,\mathrm{tw}}$: initial, first and second stiffness of tube wall E_{tw}: elastic modulus of steel ν: Poisson's ratio d_{hole}: diameter of hole D_{o}: out diameter of circular steel tube
	Anchorage	$P_{\mathrm{c,c}} = 2A_{\mathrm{brg}}^2 f_{\mathrm{c}} / A_{\mathrm{bb}}$ $P_{\mathrm{u,c}} = 16.8\sqrt{f_{\mathrm{c}}} \cdot h_{eff}^{1.5}$ $K_{0,\mathrm{c}} = \pi E_{\mathrm{c}} d_{\mathrm{bb}} / 4$ $K_{1,\mathrm{c}} = 5\% K_{0,\mathrm{c}}$	$P_{\mathrm{c,c}}$: local crushing capacity for concrete around anchor $P_{\mathrm{u,c}}$: ultimate capacity of anchorage A_{brg}: net bearing area of the head on concrete f_{c}: concrete compressive strength h_{eff}: embedment length $K_{0,\mathrm{c}}$, $K_{1,\mathrm{c}}$: initial and secondary stiffness of anchorage E_{c}: elastic modulus of concrete
Debnath and Chan 2022 [29]	Bolt shank	$F_{\mathrm{y,b}} = A_{\mathrm{b}} f_{\mathrm{y,b}}$ $F_{\mathrm{u,b}} = A_{\mathrm{b}} f_{\mathrm{u,b}}$ $K_{1,b} = A_b E_b / l_b$ $K_{2,b} = 0.08 K_{1,b}$	$F_{\mathrm{y,b}}$, $F_{\mathrm{u,b}}$: yield and ultimate strength of Hollo bolt A_{bb}: hollo bolt tensile area $f_{\mathrm{y,b}}$, $f_{\mathrm{u,b}}$: yield and ultimate strength of Hollo bolt shank material $K_{1,\mathrm{b}}$, $K_{2,\mathrm{b}}$: initial and second stiffness l_{b}: bolt shank length E_{b}: Young's modulus of bolt shank
	Tube wall bearing	$F_{\mathrm{u,tw}} = 0.7 f_{\mathrm{u,tw}} 2 d_{\mathrm{b}} t_{\mathrm{tw}}$ $F_{\mathrm{y1,tw}} == 0.4 F_{\mathrm{u,tw}}$ $F_{\mathrm{y2,tw}} = (f_{\mathrm{y,tw}} / f_{\mathrm{u,tw}}) F_{\mathrm{u,tw}}$	$F_{\mathrm{u,tw}}$: ultimate capacity of tube wall $f_{\mathrm{y,tw}}$, $f_{\mathrm{u,tw}}$: yield and ultimate strength of tube wall steel d_{b}: diameter of bolt t_{tw}: thickness of tube wall $F_{\mathrm{y1,tw}}$, $F_{\mathrm{y2,tw}}$: first and second yield capacity of tube wall

		$K_{1,\mathrm{tw}}=\dfrac{\pi E_{\mathrm{tw}}t_{\mathrm{tw}}^{2}}{4(1-\nu^{2})B}(\dfrac{2d_{\mathrm{b}}}{d_{\mathrm{hole}}})^{12}$ $K_{2,\mathrm{tw}}=0.4K_{1,\mathrm{tw}}$ $K_{3,\mathrm{tw}}=0.1K_{1,\mathrm{tw}}$	$K_{1,\mathrm{tw}}$, $K_{2,\mathrm{tw}}$, $K_{3,\mathrm{tw}}$: initial, first and second stiffness of tube wall E_{tw}: Young's modulus of steel tube d_{hole}: diameter of hole ν: Poisson's ratio B: width of tube
	Anchorage	$F_{\mathrm{c,conc}}=2A_{\mathrm{brg}}f_{\mathrm{c}}$ $F_{\mathrm{u,conc}}=16.8\sqrt{f_{\mathrm{c}}}h_{\mathrm{eff}}^{1.5}$ $K_{1,\mathrm{conc}}=\pi E_{\mathrm{c}}d_{\mathrm{b}}/4$ $K_{2,\mathrm{conc}}=0.05K_{1,\mathrm{conc}}$	$F_{\mathrm{c,conc}}$: concrete crushing strength $F_{\mathrm{u,conc}}$: pull out strength of concrete A_{brg}: net bearing area of the head on concrete f_{c}: concrete compressive strength h_{eff}: embedment length $K_{1,\mathrm{conc}}$, $K_{2,\mathrm{conc}}$: initial and second stiffness of anchorage E_{c}: elastic modulus of concrete
	Expandable sleeve	$F_{\mathrm{u,sl}}=A_{\mathrm{sl}}f_{\mathrm{u,sl}}$ $F_{\mathrm{y1,sl}}=XF_{\mathrm{u,sl}}$ $F_{\mathrm{y2,sl}}=YF_{\mathrm{u,sl}}$ $K_{1,\mathrm{sl}}=k_{\mathrm{norm}}F_{\mathrm{u,sl}}$ $K_{2,\mathrm{sl}}=\mu^{\mathrm{p}}K_{1,\mathrm{sl}}$ $K_{3,\mathrm{sl}}=\mu^{\mathrm{u}}K_{1,\mathrm{sl}}$	$F_{\mathrm{u,sl}}$: ultimate strength of expandable sleeve $F_{\mathrm{y1,sl}}$, $F_{\mathrm{y2,sl}}$: the first and second yield capacity of sleeve X: coefficients equaling to 0.25 and 0.60 for M20 grade 8.8 and M16 grade 8.8 bolts, respectively Y: coefficients equaling to 0.68 and 0.90 for M20 grade 8.8 and M16 grade 8.8 bolts, respectively $K_{1,\mathrm{sl}}$, $K_{2,\mathrm{sl}}$, $K_{3,\mathrm{sl}}$: initial, second and third stiffness k_{norm}: a coefficient equaling to 1.114 mm^{-1} and 1.091 mm^{-1} for M20 grade 8.8 and M16 grade 8.8 bolts, respectively μ^{p}: strain hardening coefficient equaling to 0.298 and 0.289 for M20 grade 8.8 and M16 grade 8.8 bolts, respectively μ^{u}: strain hardening coefficient equaling to 0.087 and 0.032 for M20 grade 8.8 and M16 grade 8.8 bolts, respectively
Agheshlui et al. 2016 [38]	Bolt	$K_{\mathrm{b}}=2E_{\mathrm{b}}A_{\mathrm{b}}/h_{\mathrm{eff}}$	K_{b}: stiffness of bolt embedded in concrete E_{b}: elastic modulus of bolt A_{b}: tensile stress area of bolt h_{eff}: effective embedment length
	Tube wall bearing	$K_{\mathrm{tf}}=\gamma D\cdot(\dfrac{s-t}{B-2t})^{-3}$ $D=\dfrac{Et^{3}}{12(1-\nu^{2})}$ $\gamma=[280.61\cdot(\dfrac{s-t}{B-2t})-18.55]\cdot10^{-6}$	K_{tf}: stiffness of tube wall D: flexural rigidity of tube face wall B: width of tube t: thickness of tube s: distance between bolt and tube side wall E: elastic modulus of tube steel
	Concrete strut	$K_{\mathrm{vs}}=E_{\mathrm{c}}d_{\mathrm{b}}\cos^{3}\theta$	ν: Poisson's ratio

		$\theta = \arctan(\frac{h_{\text{eff}}}{s-t})$	K_{vs}: vertical component of concrete strut stiffness d_{b}: bolt diameter E_{c}: elastic modulus of concrete θ: strut angle F_{iy}, initial yield capacity f_{c}': concrete compression strength
	Initial yield load	$F_{\text{iy}} = h_{\text{eff}} d_{\text{b}} f_{\text{c}}' \cos\theta \cdot (1+\frac{K_{\text{tf}}}{K_{\text{vs}}})$	
Mahmood and Tizani 2021 [88]	Tube face component	$F_{\text{p}} = \gamma_1 (F_{\text{ps}} + F_{\text{pa}})$ $F_{\text{d}} = F_{\text{p}} \cdot 1.0734 \cdot \exp(-0.178 \cdot \frac{F_{\text{pa}}}{F_{\text{ps}}})$ $\gamma_1 = (1.1L_{\text{an}} + 130)/b$ $k_{\text{i}} = \frac{E_{\text{s}} t_{eq}^3}{12\gamma_{\text{f}}(b-2t)^2(1-\nu^2)}$ $t_{\text{eq}} = 0.015 f_{\text{cu}} + 0.008L_{\text{an}} + t$	F_{p}: plastic capacity of tube face component F_{pa}: anchorage plastic capacity F_{ps}: tube plate plastic capacity determined from yield line method F_{d}: drop capacity of tube face L_{an}: embedment length b: tube width k_{i}: initial stiffness E_{s}: elastic modulus of tube steel ν: Poisson's ratio t: tube thickness γ_{f}: coefficient read from design chart f_{cu}: cubic compressive strength of concrete
Pitrakkos and Tizani 2015 [89]	Internal bolt	$k_{\text{x}}^{\text{e}} = E_{\text{b}} A_{\text{s}} / L_{\text{b}}$ For class 8.8 bolt: $k_{\text{x}}^{\text{p}} = 0.05 k_{\text{x}}^{\text{e}}$; $k_{\text{x}}^{\text{p}} = 0.1 k_{\text{x}}^{\text{e}}$ $F_{\text{y}} = 0.9F_{\text{u}}$; $F_{\text{p}} = 0.85F_{\text{u}}$; $F_{\text{pre}} = 0.15F_{\text{u}}$ For class 10.9 bolt: $k_{\text{x}}^{\text{u}} = 0.01 k_{\text{x}}^{\text{e}}$; $k_{\text{x}}^{\text{u}} = 0.015 k_{\text{x}}^{\text{e}}$ $F_{\text{y}} = 0.95F_{\text{u}}$; $F_{\text{p}} = 0.9F_{\text{u}}$; $F_{\text{pre}} = 0.25F_{\text{u}}$	k_{x}^{e}: linear-elastic bolt stiffness k_{x}^{p}, k_{x}^{u}: first and secondary stiffness F_{u}: ultimate capacity of bolt F_{y}: yield capacity of bolt F_{p}: proportional capacity of bolt F_{pre}: preload in bolt E_{b}: elastic modulus of bolt A_{s}: bolt area L_{b}: bolt elongation length
	Expanding sleeve and Anchorage	$k_{\text{x}}^{\text{e}} = k_{\text{norm}}^{\text{e}} F_{\text{u}}$; $k_{\text{x}}^{\text{p}} = \mu^{\text{p}} k_{\text{x}}^{\text{e}}$; $k_{\text{x}}^{\text{u}} = \mu^{\text{u}} k_{\text{x}}^{\text{e}}$	F_{u}: ultimate capacity of the component k_{x}^{e}: initial stiffness of the element k_{x}^{p}, k_{x}^{u}: post-limit and ultimate stiffness $k_{\text{e}}^{\text{norm}}$, μ^{p}, μ^{u}, F_1, F_2, F_3, F_4: coefficients determined from experiments.
Cabrera et al. 2020 [26]	Combined tube face wall and bolt	$F_{\text{p}} = \min(F_{\text{p,EHB}}, F_{\text{p,tube}})$ $k_{\text{i}} = 94.5t + 262.7$ $F_{\text{d}} = 1.16F_{\text{p}} + 71.7$	F_{p}: plastic capacity of the connection $F_{\text{p,EHB}}$: plastic capacity of bolt component $F_{\text{p,tube}}$: plastic capacity of tube face component t: tube thickness in mm k_{i}: initial stiffness of the connection F_{d}: drop capacity of the connection

Silva et al. 2003 [90]	Tube face	$S_{\mathrm{i}} = \frac{Et_{wc}^3}{L^2} 16 \frac{\alpha + (1-\beta)\tan\theta}{(1-\beta)^3 + 10.4 \cdot (1.5 - 1.63\beta)/\mu^2}$ $\theta = 35 - 10\beta$; $\alpha = c/L$; $\beta = b/L$	S_{i}: initial stiffness of tube face t_{wc}: tube thickness E: elastic modulus of tube steel b, c, θ, L: as illustrated in Fig. 25
Gomes et al. 1996 [91]	Tube face	$F_{\mathrm{pl,Gomes}} = \frac{4\pi m_{\mathrm{p}}}{1 - b/L}(\sqrt{1 - \frac{b}{L}} + \frac{2c}{\pi L})$ $b = g + 0.9d_{\mathrm{h}}$; $c = p + 0.9d_{\mathrm{h}}$	$F_{\mathrm{pl,Gomes}}$: plastic capacity by yield line method m_{p}: plastic moment per unit length of yield line g: bolt gauge distance p: bolt pitch distance d_{h}: equivalent diameter of bolt head L: inner width of tube $F_{\mathrm{pl,Yeomans}}$: plastic capacity by yield line method d_{b}: bolt diameter
Yeomans 1994 [92]	Tube face	$F_{\mathrm{pl,Yeomans}} = \frac{16 m_{\mathrm{p}}}{1 - b/L}(\sqrt{1 - \frac{b}{L}} + \frac{c}{2L})$ $b = g - d_{\mathrm{b}}$; $c = p - d_{\mathrm{b}}$	

4.2 Ajax anchored bolted connection to CFST

4.2.1 Component method

Oktavianus et al. [39] proposed a component model for pullout behavior of headed anchored blind bolt connected to circular CFSTs and this model was also applicable for rectangular CFSTs with minor modifications. The connection was consisted of four components, namely free blind-bolt, steel tube wall, embedded bolt shank and embedded head, and each component was modeled by a spring with multilinear load-displacement response (Fig. 20). The overall load-displacement response could then be obtained by assembling the springs.

As shown in Fig. 20, the tensile behavior of bolt shank (i.e., component 1 and 3) was modeled by a trilinear model based on material properties of bolt steel and ignoring the bonding stress. The spring for bearing effect was modeled by a quad-linear model. The ultimate capacity $P_{u,tw}$ of tube bearing was predicted by modifying the design equations of screw connections in AISI [93], which depended on the ultimate strength of tube, nut size and tube thickness. The yield capacity $P_{y2,tw}$ and the proportional capacity $P_{y1,tw}$ are associated with $P_{u,tw}$ and the ultimate-to-yield strength ratio of steel tube. The initial stiffness $K_{0,tw}$ was derived from plate theory and $K_{1,tw}$ is set as $0.2K_{0,tw}$ and $K_{2,tw}$=$0.06K_{0,tw}$. The anchorage was simulated by a trilinear model whose yield capacity $P_{c,c}$ corresponded to a concrete crush at the root of anchor and the ultimate capacity $P_{u,c}$ was associated to the formation of the concrete cone. The initial stiffness $K_{0,c}$ was assumed to be related the annular concrete around bolt shank and the secondary stiffness is set as $0.05K_{0,c}$. After knowing the response of each components, the overall load-displacement relationship could then be predicted, which showed a good match with experimental and FE curves.

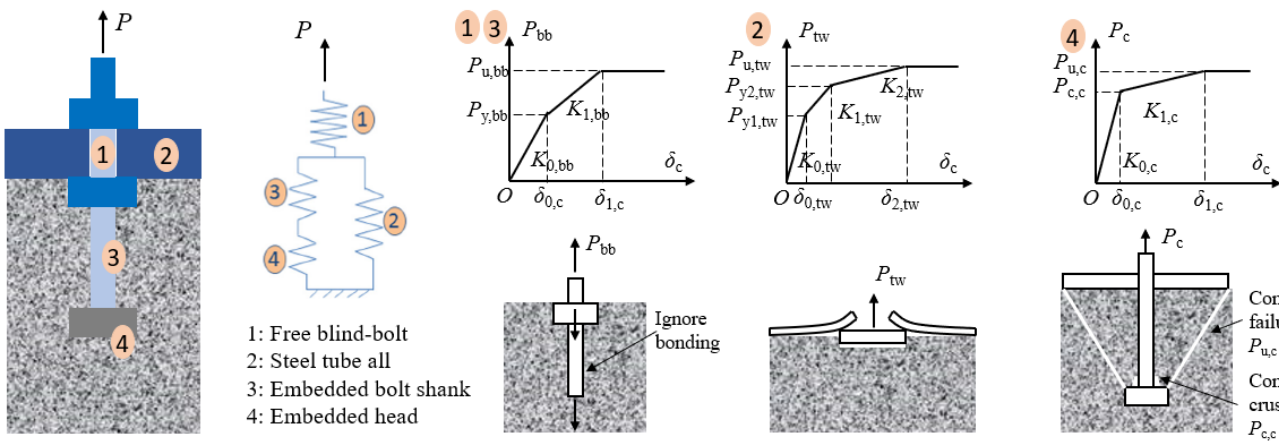

Fig. 20 Component method in Oktavianus et al. 2017 [39]: (a) component; (b) spring assembly; (c) bolt shank model; (d) tube bearing model; (e) anchorage model.

4.2.2 Strut and tie model

Based experimental results, Agheshlui et al. [38] concluded that a concrete strut was formed as shown in Fig. 21(a) if the bolt was located near the tube side wall. A strut-and-tie model was proposed to predict the load-displacement response up to $0.6F_u$, in which F_u is the nominal capacity of bolt. The cross-section of concrete strut was assumed to be rectangular with width equaling to half of embedment length and thickness equaling to bolt diameter. A spring assembly was constructed to estimate the connection stiffness, which was contributed by the tube bearing K_{tf}, bolt elongation K_b and the vertical component of concrete strut K_{vs} (Fig. 21(b)), among which K_{tf} was related to the plate stiffness and the location of bolt and K_{vs} was governed by the concrete strut stiffness and strut angle. The yield capacity F_{iy} corresponded to the damage initiation in the concrete strut and the stress in the concrete strut at F_{iy} was assumed as the concrete strength. The strut-and-tie model exhibited an acceptable accuracy as demonstrated in Agheshlui et al. [38].

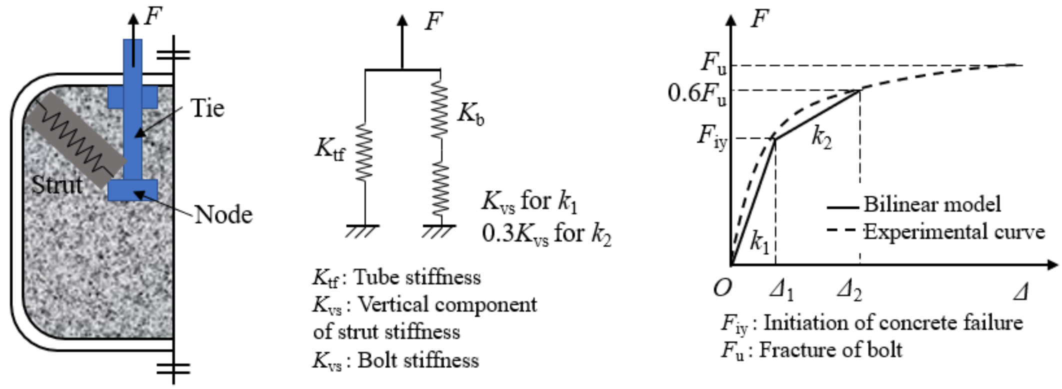

(a) (b) (c)

Fig. 21 Strut and tie model (Agheshlui et al. 2016 [38]): (a) Strut and tie mode; (b) Springs for stiffness calculation; (c) Load-displacement model

4.3 EHB connection to CFST

4.3.1 Model for tube face wall component

Mahmood and Tizani [88] proposed a quad-linear model for column face bending in EHB connections. Both the effects of tube face wall and anchorage were considered in the model. Because the effect of bolt was not included in the model, it was referred as a model for tube face wall instead of the whole connection. It should be emphasized that the tube face wall behaved differently from that will be discussed in Section 4.4 in which the anchorage effect did not exist.

As shown in Fig. 22(a), key parameters in the quad-linear model includes the plastic capacity F_p, the initial stiffness k_i and the drop load F_d. The plastic capacity was the summation of the resistances provided by the tube (F_{ps}) and the anchorage (F_{pa}), multiplied by a geometry coefficient (γ_1). The plastic capacity of tube face wall was determined by the yield line method. Fig. 22(b) shows the possible yield line patterns for a tube face wall with four bolts and the minimum load of them was adopted as F_{ps}. The anchorage capacity was assumed to equal to the confined concrete strength multiplied by the projected area of the concrete cone. Similarly, different patterns of concrete cone might exist and the minimum resistance was taken as F_{pa}. The initial stiffness was derived from plate stiffness theory. An equivalent thickness was defined for the tube to consider the influences of concrete infill and the anchorage. In addition, a deflection coefficient related to bolt gauge and tube size was introduced for the determination of k_i and it could be read from an empirical chart. Calculation of the F_d was based on a formula in [94]. Performance of the proposed model was assessed by comparing with the experiment results showing an acceptable accuracy [88].

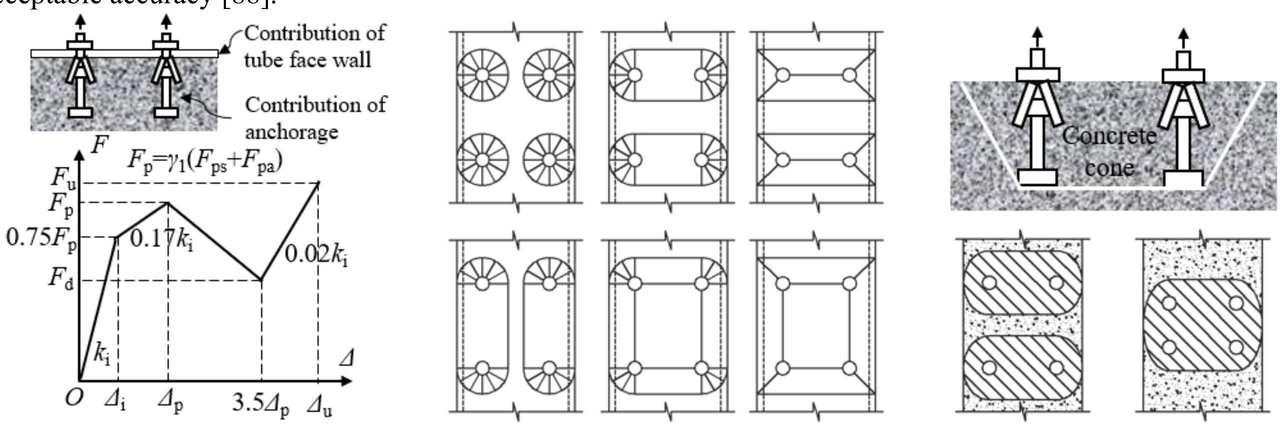

(a) (b) (c)

Fig. 22 Component model for tube face wall in an EHB connection (Mahmood and Tizani 2021 [88]): (a) quad-linear model; (b) yield line pattern of steel face wall for F_{ps}; (c) concrete anchorage cone for F_{pa}.

4.3.2 Model for EHB

Based on experimental results in Pitrakkos and Tizani [48], Pitrakkos and Tizani [89] proposed a component method for EHB embedded in concrete. The bolt was divided into three elements, i.e., internal bolt, expanding sleeve and anchorage (Fig. 23 (a)). It is necessary to mention that the tube face wall was rigid and not considered in the model. Each element was modeled by a multilinear spring and they were assembled to represent the bolt behavior as shown in Fig. 23 (b). The load-displacement model for the internal bolt contained four segments that were divided by the preload F_{pre}, proportional load F_{p}, yield capacity F_{y} and ultimate capacity F_{u} (Fig. 23(c)). The parameters in the model depended on the bolt grade (e.g., class 8.8 or 10.9). Trilinear model shown in Fig. 23(d) was adopted for the expanding sleeve and anchorage. The parameters needed in the model for sleeve and anchorage were obtained from experimental results. The prediction matched well with their previous experimental results.

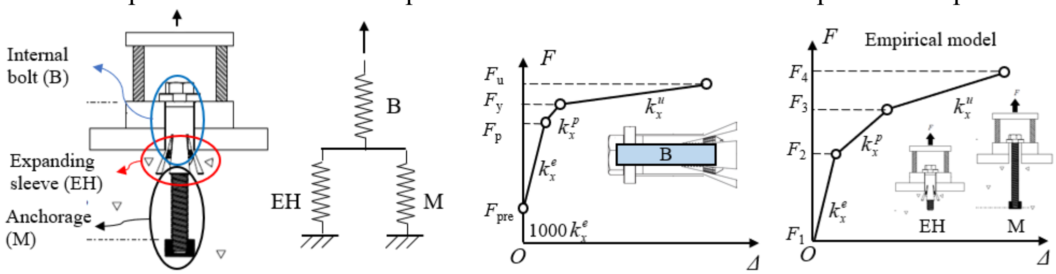

Fig. 23 Component method for EHB in concrete (Pitrakkos and Tizani 2015 [89]): (a) elements in EHB; (b) spring model; (c) load-displacement model for internal bolt; (d) load-displacement model for expanding sleeve and anchorage.

4.3.3 Model for EHB connection to CFST

Based on the studies on EHB component and tube face wall component introduced in Section 4.3.1 and 4.3.2, Cabrera et al. [26] proposed a quad-linear model for EHB connected to CFSTs as shown in Fig. 24. The plastic resistance F_{p} is taken as the minimum resistances of bolt and tube face wall components. The initial stiffness was determined by an empirical equation which depended on tube thickness (t in mm). In this empirical model, some of the parameters were specified by regression analysis on experimental and FE results.

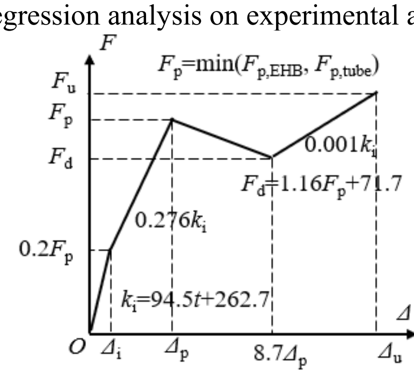

Fig. 24 Model for EHB connection to CFST (Cabrera et al. 2020 [26]).

Debnath and Chan [29] proposed a component method for EHB connected to CFSTs and the system included five components as shown in Fig. 25(a). Comparing to the component method in Oktavianus et al. [39], an "expandable sleeve" component was established for EHB. The free bolt part and embedded bolt part were modeled by a trilinear model. The length of bolt shank (l_{b}) for free bolt part is calculated by Eq. (2) and the length for embedded bolt part is l_{emb}

$$l_{\mathrm{b}} = t_{\mathrm{bc}} + t_{\mathrm{ep}} + t_{\mathrm{tw}} + t_{\mathrm{cn}} \quad (2)$$

where t_{bc}, t_{ep}, t_{tw}, l_{cn} and l_{emb} are illustrated in Fig. 25(b). The tri-linear model in Pitrakkos and Tizani [89] was adopted for the expandable sleeve part and the coefficients in the model were determined by experiments. A quad-linear model was constructed for the tube wall component. A new formula was proposed to consider the unique interlocking mechanism of Hollo bolt to the tube wall. For concrete anchorage, a trilinear model was adopted. As verified by experimental results, the proposed component method provided an accurate prediction on the load-displacement response of EHB connected to CFSTs.

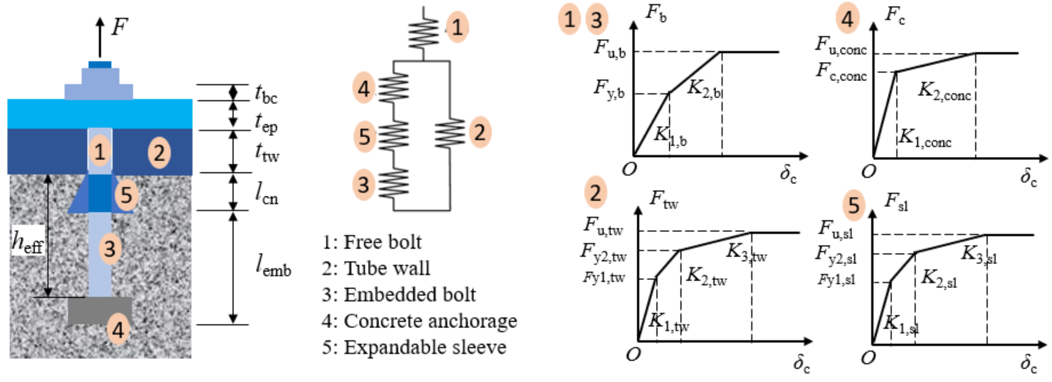

(a) (b) (c)

Fig. 25 Component model for EHB connected to CFSTs (Debnath and Chan 2022 [29]): (a) components; (b) spring assembly; (c) load-displacement model.

4.4 Model for tube face wall

4.4.1 Initial stiffness

Behavior of tube face wall plays an important role in a blind bolted connection. In general, plate theory and beam theory were widely used for the determination of the initial stiffness. In the plate theory, the initial stiffness was related to the flexural rigidity and empirical coefficients were adopted to account for the effect of concrete infill and the discrepancy between theoretical and experimental results [38, 39, 88]. On the other hand, the beam theory assumed the tube face wall as a beam (i.e., one-way slab) with effective width L_{eff}. The boundary condition for the beam was commonly set as a fixed support or a semi-fixed support (e.g., rotation spring support). Silva et al. [90] proposed a method to calculate the initial stiffness of the tube face wall as shown in Fig. 26. The area surrounded by the four bolts was assumed as rigid and the effective width L_{eff} depended on the angle θ that was related to bolt gauge-to-tube width ratio. The initial stiffness was then calculated with the considerations on both flexural and shear deformations.

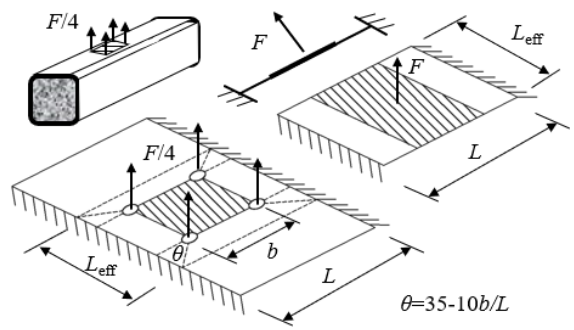

Fig. 26 Beam theory for initial stiffness calculation (Silva et al. 2003 [90])

4.4.2 Resistance

Yield line method was widely used for steel members and connections that involved local collapse mechanisms [95]. The yield line method was also adopted to predict the plastic resistance of the tube face wall, such as CIDECT Design Guide No. 9 [14], Wang et al. [9] and Mahmood and Tizani [88]. Two typical yield line methods are illustrated in Fig. 27 with different yield line patterns, namely Gomes method [91] and Yeomans method [92]. The corresponding plastic resistance was calculated in Eqs. (3) and (4) respectively:

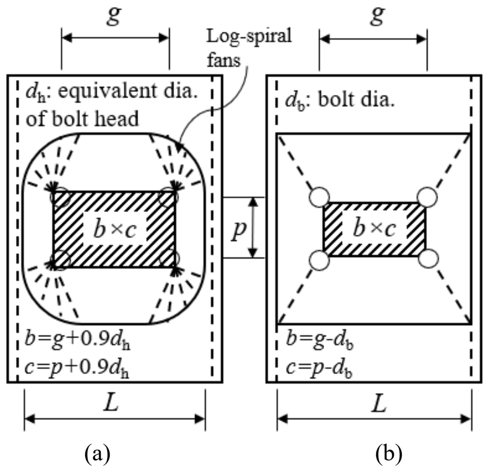

Fig. 27 Yield line method: (a) Gomes method (Gomes et al. 1996 [91]); (b) Yeomans method (Yeomans 1994 [92]).

$$F_{\text{pl,Gomes}} = \frac{4\pi m_{\text{p}}}{1-b/L}\left(\sqrt{1-\frac{b}{L}}+\frac{2c}{\pi L}\right) \quad (3)$$

$$F_{\text{pl,Yeomans}} = \frac{16 m_{\text{p}}}{1-b/L}\left(\sqrt{1-\frac{b}{L}}+\frac{c}{2L}\right) \quad (4)$$

where m_p is the plastic moment per unit length of yield line. Although the formats of Eqs. (3) and (4) are quite similar, the plastic resistances calculated by them show great difference because the definition of the rigid area (i.e., $b \times c$) in Fig. 27 is different. Based on beam theory, Li and Zhao [22] proposed a load-displacement model for stainless steel tube face wall. The model consisted of an exponential first portion and a straight line second portion.

5. Conclusions

This paper presented a critical review on the blind bolted connections to CFSTs, including experimental, FE and theoretical studies. Behaviors of a single bolt or bolt group connected to CFSTs and their individual components were discussed. The following conclusions could be drawn:

(1) For an anchored blind bolted connection to CFST, the strength and stiffness are mainly contributed by the anchorage, bolt shank elongation and tube bearing. The contributions of these components might be influenced interactively. The tube not only provides bearing force on bolt but also restrains the concrete deformation that may indirectly contribute to the anchorage. Apart from anchoring effect, the concrete also resists the inward deformation of steel tube face wall leading to a change of its boundary conditions.

(2) For Hollo bolt and its variants, the interlocking between bolt and steel tube wall is complex involving the inclined sleeves and the concrete between the sleeves and tube wall. The inner nut surfaces of Ajax bolt, T-bolt and their variants are flat and could be bore on the steel tube wall. Owing to the different interlocking mechanisms and anchor shapes, the behavior of connections with different anchored blind bolt types varied greatly.

(3) Enhancement in strength and stiffness by setting an anchor has been experimentally confirmed and widely accepted. The significance of adding a second anchor seems not reach a consensus probably due to the different types of anchors used in the research.

(4) Failure modes of a tensile connection could be pullout of bolt, anchorage failure in concrete, bolt fracture, excessive yielding of steel tube or tube hole tearing, which depends on the relative strength contributed by the anchorage, bolt and tube.

(5) Performance of a connection depends on various parameters, such as bolt type, bolt size, bolt grade, quantity of anchors, embedment length, concrete strength, steel yield strength, tube width (or diameter)-to-thickness ratio, and bolt layout (i.e., gauge and pitch for bolt group).

(6) FE is a powerful tool for parametrical study and understanding the stress distribution in a connection. Nevertheless, a reliable modeling of concrete is important due to the complex interactions between concrete and the embedded bolts. Concrete damage model is recommended to model the concrete.

(7) Various models have been proposed for anchored blind bolted connection to CFSTs. Nevertheless, some parameters in these models were determined from experiments, which hinders a more versatile application of these models.

6. Applications and suggestions for future study

Blind bolts have been successfully applied to steel hollow sectional structures, to name a few examples, Hollo bolts for the CHS posts in Bahrain airport project and the modules in citizenM Hotel project [96]; One-side bolts for towers [97]. In addition, the blind bolting method has been covered in some design guidelines for hollow section structures (e.g., CIDECT). Flowdrill system, Lindadpter Hollo bolt and Huck Ultra-Twist system were recommended in CIDECT. However, to the authors' best knowledge, the application of blind bolts for CFST structures is seldomly reported. The possible reasons and challenges for promoting blind bolted connections in CFST structures include: 1) Blind bolting is a new technique for CFST structures and has not been widely accepted by the industry; 2) The blind bolted joint is semirigid and the structural analysis is more complex than structures adopting rigid or pined joints; 3) It is still lack of experimental studies on large-scale joints and demonstration projects.

Although extensive research has been conducted for blind bolted connections to CFSTs during the last ten years, the following topics are suggested for future studies:

(1) Interaction effect between tube, concrete and bolt needs to be further clarified. Component method is a powerful approach to analyze the connection behavior but the correlation between components also deserves more attentions. For example, the tube not only provides bearing strength but also restrains the deformation of concrete cone and enhances the concrete strength by offering confinement.

(2) For a design purpose, the stiffness and strength are most important. Consensus has not been reached regarding the maximum strength and deformation a blind bolted connection could be utilized.

(3) Only very limited studies touched the cyclic behavior of the connection. Degradation of the anchorage and the preload due to cyclic (or seismic) loads needs further research.

(4) It is known that the preload plays an important role in connection behavior. Effects of preload on the performance of blind bolted connection (i.e., stiffness and deformability) should be further investigated.

(5) Although various theoretical models have been proposed, most of them were quite empirical and were not verified by the experimental results from other researchers. Research is needed to develop unified and versatile models.

(6) Existing anchored blind bolts still had some disadvantages when used in engineering practice and the stiffness is a major concern if comparing to welded CFST joints widely used in real projects. It is expected to further improve the performance of the anchored blind bolts or even invent new jointing techniques.

(7) Only a few studies were conducted for anchored blind bolts under combined tensile and shear loads, and the research on circular CFST connection is rather limited as well. Bolts in the tension zone of a beam-to-column joint are commonly under combined actions and the circular CFST is widely used in engineering practice. Therefore, more research is required for these aspects.

(8) The pullout test aims to simulate the tensile zone in a beam-to-column joint. However, it is still lack of studies to corelate the tensile behavior of the tension zone to the overall moment-rotation behavior of a beam-to-column joint.

(9) Concrete-filled double-skin steel tube (CFDST) is an efficient cross-section type for columns that attracted researchers' attention in recent years [10]. It is lack of studies on the blinded bolted connections to CFDSTs. Effects of the inner steel tube and void ratio on the connection behavior need to be clarified.

Acknowledgements

The first author's postdoctoral fellowship is sponsored by the Innovation and Technology Fund (ITF) – Research Talent Hub. The authors are grateful to the financial support provided by the Chinese National Engineering Research Centre for Steel Construction (Hong Kong Branch).

References

[1] Y.-L. Li, X.-L. Zhao, Experimental study on stainless steel blind bolted T-stub to square hollow section connections, Thin-Walled Struct 167 (2021) 108259.

[2] Lindapter, Lindapter Hollobolt, 2022. http://www.lindapter.com/Products/Hollo-Bolt_And_Lindibolt/2. (Accessed 18/6/2022 2022).

[3] MolaBolt, MolaBolt, 2022. https://molabolt.co.uk/. (Accessed 18/6/2022 2022).

[4] Howmet, Huck blind fasteners, 2022. https://www.hfsindustrial.com/us/huck. (Accessed 18/6/2022 2022).

[5] Ajax, Ajax fasteners: the ultimate high strength structural blind fastening system., 2022. https://pdf4pro.com/amp/cdn/x-y-r-blind-fastening-system-ajax-fasteners-1818a8.pdf. (Accessed 18/6/2022 2022).
[6] BlindBolt, Blind bolt, 2022. https://www.blindbolt.co.uk/. (Accessed 18/6/2022 2022).
[7] W. Wang, L. Li, D. Chen, Progressive collapse behaviour of endplate connections to cold-formed tubular column with novel Slip-Critical Blind Bolts, Thin-Walled Struct 131 (2018) 404-416.
[8] W. Tizani, D. Ridley-Ellis, The performance of a new blind-bolt for moment-resisting connections, in: M.A. Jaurietta, A. Alonso, J.A. Chica (Eds.) the 10th International Symposium on Tubular Structures, Routledge, Madrid, Spain, 2003, pp. 395-400.
[9] P. Wang, L. Sun, B. Zhang, X. Yang, F. Liu, Z. Han, Experimental studies on T-stub to hollow section column connection bolted by T-head square-neck one-side bolts under tension, J Constr Steel Res 178 (2021) 106493.
[10] X.L. Zhao, L.H. Han, H. Lu, Concrete-filled tubular members and connections, Taylor & Francis, London, 2010.
[11] Z. Chen, Y. Qin, X. Wang, Development of connections to concrete-filled rectangular tubular columns, Advanced Steel Construction 11(4) (2015) 408-426.
[12] Z.-B. Wang, Z. Tao, D.-S. Li, Lin-HaiHan, Cyclic behaviour of novel blind bolted joints with different stiffening elements, Thin-WalledStructures 101 (2016) 157–168.
[13] H. Yao, H. Goldsworthy, E. Gad, Experimental and numerical investigation of the tensile behavior of blind-bolted T-stub connections to concrete-filled circular columns, J Struct Eng 134(2) (2008) 198-208.
[14] Y. Kurobane, J.A. Packer, J. Wardenier, N. Yeomans, Design Guide for Structural Hollow Section Column Connections, Verlag TUV Rheinland, Cologne, Germany, 2004.
[15] ACI318-11, Building code requirements for structural concrete and commentary, American Concrete Institute, Farmington Hills, MI, 2011.
[16] M. Cabrera, W. Tizani, J. Ninic, A review and analysis of testing and modeling practice of extended Hollo-Bolt blind bolt connections, J Constr Steel Res 183 (2021) 106763.
[17] W. Tizani, M. Cabrera, M. Mahmood, J. Ninic, F. Wang, The behaviour of anchored extended blind bolts in concrete-filled tubes, Steel Construction 15(S1) (2022) 51–58.
[18] M.Z. Jeddi, N.R. Sulong, Pull-out performance of a novel anchor blind bolt (TubeBolt) for beam to concrete-filled tubular (CFT) column bolted connections, Thin-Walled Struct 124 (2018) 402-414.
[19] H. Yao, H. Goldsworthy, E. Gad, S. Fernando, Experimental study on modified blind bolts anchored in concrete-filled steel tubular columns, Australian earthquake engineering society 2011 conference, Barossa Valley, Australia, 2011.
[20] Y. Oktavianus, H.M. Goldsworthy, E.F. Gad, Cyclic behaviour of individual double headed anchored blind bolts within CFST, J Constr Steel Res 133 (2017) 522-534.
[21] L. Sun, Z. Liang, L. Wu, C. Li, Y. Liu, M. Liu, F. Liu, P. Wang, Experimental and theoretical modeling for predicting bending moment capacity of T-head square-neck one-side bolted endplate to tube column connection, J Build Eng 43 (2021) 103104.
[22] Y.-L. Li, X.-L. Zhao, Study on stainless steel blind bolted T-stub to concrete-filled stainless steel tube connections, Eng Struct 257 (2022) 114107.
[23] E.L. Tan, H. Varsania, F. Liao, Experimental study on demountable steel-concrete connectors subjected to combined shear and tension, Eng Struct 183 (2019) 110–123.
[24] T. Pitrakkos, The tensile stiffness of a novel anchored blind-bolt component for moment-resisting connections to concrete-filled hollow sections, University of Nottingham, 2012.
[25] T. Pitrakkos, W. Tizani, M. Cabrera, N.F. Salh, Blind bolts with headed anchors under combined tension and shear, J Constr Steel Res 179 (2021) 106546.
[26] M. Cabrera, W. Tizani, M. Mahmood, M.F. Shamsudin, Analysis of Extended Hollo-Bolt connections: Combined failure in tension, J Constr Steel Res 165 (2020) 105766.
[27] P.P. Debnath, T.-M. Chan, A comprehensive numerical approach for modelling blind-bolted CFST connections, Struct 33 (2021) 2208-2225.
[28] P.P. Debnath, T.-M. Chan, Tensile behaviour of headed anchored hollo-bolts in concrete filled hollow steel tube connections, Eng Struct 234 (2021) 111982.
[29] P.P. Debnath, T.-M. Chan, Experimental evaluation and component model for single anchored blind bolted concrete filled tube connections under direct tension, J Constr Steel Res 196 (2022) 107391.

[30] P.P. Debnath, T.-M. Chan, Experimental performance of single blind-bolted CFST column connection under predominant shear loading, J Constr Steel Res 196 (2022) 107386.
[31] W. Tizani, N. Abd Rahman, T. Pitrakkos, Fatigue life of an anchored blind-bolt loaded in tension, J Constr Steel Res 93 (2014) 1-8.
[32] A.M. Pascual, M.L. Romero, W. Tizani, Fire performance of blind-bolted connections to concrete filled tubular columns in tension, Eng Struct 96 (2015) 111-125.
[33] A.M. Pascual, M.L. Romero, W. Tizani, Thermal behaviour of blind-bolted connections to hollow and concrete-filled steel tubular columns, J Constr Steel Res 107 (2015) 137-149.
[34] M. Cabrera, W. Tizani, J. Ninic, F. Wang, Experimental and numerical analysis of preload in Extended Hollo-Bolt blind bolts, J Constr Steel Res 186 (2021) 106885.
[35] W. Tizani, T. Pitrakkos, Performance of T-stub to CFT joints using blind bolts with headed anchors, J Struct Eng 141(10) (2015) 04015001.
[36] Y. Oktavianus, H. Yao, H.M. Goldsworthy, E.F. Gad, Pull-out behaviour of blind bolts from concrete-filled tubes, Proceedings of the Institution of Civil Engineers-Structures and Buildings 168(10) (2015) 747-759.
[37] H. Agheshlui, H. Goldsworthy, E. Gad, S. Fernando, Tensile behaviour of anchored blind bolts in concrete filled square hollow sections, Materials and Structures 49(4) (2016) 1511-1525.
[38] H. Agheshlui, H. Goldsworthy, E. Gad, H. Yao, Tensile behavior of groups of anchored blind bolts within concrete-filled steel square hollow sections, J Struct Eng 142(2) (2016) 04015125.
[39] Y. Oktavianus, H. Chang, H.M. Goldsworthy, E.F. Gad, Component model for pull-out behaviour of headed anchored blind bolt within concrete filled circular hollow section, Eng Struct 148 (2017) 210-224.
[40] T. Pokharel, H.M. Goldsworthy, E.F. Gad, Tensile behaviour of double headed anchored blind bolt in concrete filled square hollow section under cyclic loading, Constr Build Mater. 200 (2019) 146-158.
[41] Y. Oktavianus, H.M. Goldsworthy, E. Gad, Group behavior of double-headed anchored blind bolts within concrete-filled circular hollow sections under cyclic loading, J Struct Eng 143(10) (2017) 04017140.
[42] T. Pokharel, H.M. Goldsworthy, E.F. Gad, Tensile behavior of groups of double-headed anchored blind bolts within concrete-filled square hollow sections under cyclic loading, J Struct Eng 147(3) (2021) 04020349.
[43] L. Sun, Z. Liang, Q. Wang, H. Zhu, P. Wang, Y. Liu, F. Liu, Seismic response on T-head square-neck one-side bolted endplate connection of beam to square tubular column, Eng Struct 246 (2021) 113077.
[44] W.H. Ng, S.Y. Kong, Y.S. Chua, Y. Bai, Tensile behaviour of innovative one-sided bolts in concrete-filled steel tubular connections, J Constr Steel Res 191 (2022) 107165.
[45] A.M.E.A. Elamin, The face bending behaviour of blind-bolted connections to concrete-filled hollow sections, University of Nottingham, 2014.
[46] M. Mahmood, W. Tizani, C. Sansour, Effect of tube thickness on the face bending for blind-bolted connection to concrete filled tubular structures, International Journal of Civil, Architectural, Structural and Construction Engineering 8(9) (2014) 897-903.
[47] W. Tizani, M. Mahmood, D. Bournas, Effect of concrete infill and slenderness on column-face component in anchored blind-bolt connections, J Struct Eng 146(4) (2020) 04020041.
[48] T. Pitrakkos, W. Tizani, Experimental behaviour of a novel anchored blind-bolt in tension, Eng Struct 49 (2013) 905-919.
[49] KYOWA, Strain gages for measuring axial tension of bolts, 2022. https://www.kyowa-ei.com/eng/product/category/strain_gages/kfb/index.html. (Accessed 18/6/2022 2022).
[50] J. Lee, H. Goldsworthy, E. Gad, Blind bolted T-stub connections to unfilled hollow section columns in low rise structures, J Constr Steel Res 66(8-9) (2010) 981-992.
[51] N.S. Welding, Embedment properties of headed studs, Design data 10, Nelson Division, Lorain, OH, 1974.
[52] M.N. Amin, S. Zaheer, A.A. Alazba, M.U. Saleem, M.U.K. Niazi, N. Khurram, M.T. Amin, A component-based study of the effect of diameter on bond and anchorage characteristics of blind-bolted connections, Plos One 11(2) (2016) e0149490.
[53] J.-F. Wang, L.-H. Han, B. Uy, Behaviour of flush end plate joints to concrete-filled steel tubular columns, J Constr Steel Res 65 (2009) 925939.
[54] J.-F. Wang, L.-H. Han, B. Uy, Hysteretic behaviour of flush end plate joints to concrete-filled steel tubular columns, J Constr Steel Res 65 (2009) 1644-1663.
[55] Z. Tao, M.K. Hassan, T.-Y. Song, L.-H. Han, Experimental study on blind bolted connections to concrete-filled stainless steel columns, J Constr Steel Res 128 (2017) 825-838.

[56] W. Tizani, A. Al-Mughairi, J.S. Owen, T. Pitrakkos, Rotational stiffness of a blind-bolted connection to concrete-filled tubes using modified Hollo-bolt, J Constr Steel Res 80 (2013) 317-331.
[57] W. Tizani, Z.Y. Wang, I. Hajirasouliha, Hysteretic performance of a new blind bolted connection to concrete filled columns under cyclic loading: An experimental investigation, Eng Struct 46 (2013) 535-546.
[58] L. Sun, M. Liu, Y. Liu, P. Wang, H. Zhao, J. Sun, Y. Shang, Studies on T-shaped one-side bolted connection to hollow section column under bending, J Constr Steel Res 175 (2020) 106359.
[59] C. Wan, Y. Bai, C. Ding, L. Zhu, L. Yang, Mechanical performance of novel steel one-sided bolted joints in shear, J Constr Steel Res 165 (2020) 105815.
[60] A.M.E.A. Elamin, The face bending behaviour of blind-bolted connections to concrete-filled hollow sections, University of Nottingham, 2014.
[61] M. Mahmood, W. Tizani, C. Sansour, Effect of tube thickness on the face bending for blind-bolted connection to concrete filled tubular structures, International Journal of Civil, Architectural, Structural and Construction Engineering 8(9) (2014) 904-910.
[62] E. 1993-1-2, Design of steel structures - Part 1-2: General rules - Structural fire design, European Committee for Standardization, Brussels, 2005.
[63] Y. You, M. Liu, Y. Liu, P. Wang, S. Zhou, J. Chen, Experimental studies on thread-fixed one-side bolted T-stubs in tension at elevated temperatures, J Constr Steel Res 171 (2020) 106139.
[64] Y. You, H. Zhu, X. Liu, C. Xia, M. Liu, Y. Liu, F. Liu, Post fire tensile behavior of thread-fixed one-side bolt strengthened by backing plate, Eng Struct 252 (2022) 113577.
[65] P. Wang, Y. You, Q. Wang, H. Gu, G. Wang, Y. Liu, F. Liu, Post-fire tensile behavior of hole-anchored bolted T-stub connection, J Constr Steel Res 187 (2021) 106941.
[66] T.-Y. Song, Z. Tao, A. Razzazzadeh, L.-H. Han, K. Zhou, Fire performance of blind bolted composite beam to column joints, J Constr Steel Res 132 (2017) 29–42.
[67] SIMULIA, ABAQUS, 2016.
[68] SIMULIA, Abaqus user's manual, 2016.
[69] Z. Tao, Z.-B. Wang, Q. Yu, Finite element modelling of concrete-filled steel stub columns under axial compression, J Constr Steel Res (89) (2013) 121–131.
[70] S. Popovics, A numerical approach to the complete stress-strain curve of concrete, Cem Concr Res 3(5) (1973) 583-599.
[71] E.C.f. Standardization, Eurocode 2: Design of concrete structures - Part 1-1: General rules and rules for buildings, European Committee for Standardization, Brussels, 2004.
[72] GB50010-2010, Code for design of concrete structures, China Architecture & Building Press, Beijing, China, 2015.
[73] J.B. Mander, M.J. Priestley, R. Park, Theoretical stress-strain model for confined concrete, J Struct Eng 114(8) (1988) 1804-1826.
[74] L.-H. Han, G.-H. Yao, Z. Tao, Performance of concrete-filled thin-walled steel tubes under pure torsion, Thin-Walled Struct (45) (2007) 24-36.
[75] A. Hillerborg, M. Modéer, P.-E. Petersson, Analysis of crack formation and crack growth in concrete by means of fracture mechanics and finite elements, Cem Concr Res 6(6) (1976) 773-781.
[76] B.S. Institution, Design of concrete structures, London, 1993.
[77] B. Trunk, F. Wittmann, Experimental investigation into the size dependence of fracture mechanics parameters, Third International Conference of Fracture Mechanics of Concrete Structures, Gifu, Japan, 1998, pp. 1937–1948.
[78] I.F.f.S. Concrete, Constitutive modelling for high strength/high performance concrete, Lausanne, Switzerland, 2008.
[79] MC2010, CEB-FIB model code - Final draft, Lausanne, Switzerland, 2010.
[80] T. Jankowiak, T. Lodygowski, Identification of parameters of concrete damage plasticity constitutive model, Foundations of Civil and Environmental Engineering 6 (2005) 53–69.
[81] R. Waqas, B. Uy, H.-T. Thai, Experimental and numerical behaviour of blind bolted flush endplate composite connections, J Constr Steel Res 153 (2019) 179-195.
[82] V. Birtel, P. Mark, Parameterised finite element modelling of RC beam shear failure, ABAQUS users' conference, Massachusetts, USA, 2006, pp. 95-108.
[83] B.P. Sinha, K.H. Gerstle, L.G. Tulin, Stress-strain relations for concrete under cyclic loading, Journal Proceedings 61(2) (1964) 195-212.

[84] S. Okamoto, S. Shiomi, K. Yamabe, Earthquake resistance of prestressed concrete structures, Annual Architectural Institute of Japan (AIJ) Convention, Japan, 1976, pp. 1251-1252.
[85] Y. Tanigawa, Y. Uchida, Hysteretic characteristics of concrete in the domain of high compressive strain, Annual Architectural Institute of Japan (AIJ) Convention, Japan, 1979, pp. 449-450.
[86] B.Y. Bahn, C.T.T. Hsu, Stress-strain behavior of concrete under cyclic loading, ACI Materials Journal 95 (1998) 178-193.
[87] A. Hillerborg, The theoretical basis of a method to determine the fracture energy GF of concrete, Materials and Structures 18(4) (1985) 291 - 296.
[88] M. Mahmood, W. Tizani, A component model for column face in bending of extended HolloBolt connections, J Constr Steel Res 182 (2021) 106655.
[89] T. Pitrakkos, W. Tizani, A component method model for blind-bolts with headed anchors in tension, Steel Compos Struct 18(5) (2015) 1305-1330.
[90] L. Silva, L. Neves, F. Gomes, Rotational stiffness of rectangular hollow sections composite joints, J Struct Eng 129(4) (2003) 487-494.
[91] F. Gomes, J.P. Jaspart, R. Maquoi, Moment capacity of beam-to-column minor-axis joints, IABSE Colloquium on Semi-Rigid Structural Connections, Istanbul, Turkey, 1996.
[92] N.F. Yeomans, I-beam/rectangular hollow section column connections using the Flowdrill system, in: P. Grundy, A. Holgate, B. Wong (Eds.) the 6th International Symposium on Tubular Structures, Routledge, Melbourne, Australia, 1994.
[93] A.I.a.S. Institute, North American specification for the design of cold-formed steel structural members, Washington, D.C., 2016.
[94] M.S. Mahmood, Column face bending of anchored blind bolted connections to concrete filled tubular sections, University of Nottingham, 2015.
[95] X.-L. Zhao, Yield line mechanism analysis of steel members and connections, Progress in Structural Engineering and Materials 5 (2003) 252–262.
[96] Lindapter, Case studies, 2022. https://www.lindapter.com/us/case-studies. (Accessed 24/10/2022.
[97] Allfasteners, NexGen2® Structural Blind Bolt Assembly, 2022. https://www.allfasteners.com.au/nexgen2-structural-blind-bolt-assembly.